Oceanographic Processes Driving Low Oxygen Conditions Inside Patagonian Fjords

Pamela Linford[1,2,3], Iván Pérez-Santos[2,3,4,*], Paulina Montero[3,4], Patricio Díaz[2,5], Claudia Aracena[6,7], Elías Pinilla[8,14], Facundo Barrera[9,10], Manuel Castillo[11], Aida Alvera-Azcárate[12], Mónica Alvarado[13], Gabriel Soto[8], Cécile Pujol[12], Camila Schwerter[2], Sara Arenas-Uribe[2], Pilar Navarro[2], Guido Mancilla-Gutiérrez[2], Robinson Altamirano[2], Javiera San Martín[8], Camila Soto-Riquelme[8].

[1]Programa de Doctorado en Ciencias, Mención Conservación y Manejo de Recursos Naturales, Universidad de Los Lagos, Puerto Montt, Chile.

[2]Centro i-mar, Universidad de Los Lagos, Casilla 557, Puerto Montt, Chile.

[3]Center for Oceanographic Research COPAS Sur-Austral and COPAS COASTAL, Universidad de Concepción, Chile.

[4]Centro de Investigación en Ecosistemas de la Patagonia (CIEP), Coyhaique, Chile.

[5]CeBiB, Universidad de Los Lagos, Casilla 557, Puerto Montt, Chile.

[6]Centro de Investigación en Recursos Naturales y Sustentabilidad, Universidad Bernardo O'Higgins, Avenida Viel 1497, Santiago, Chile.

[7]Laboratorio Costero de Recursos Acuáticos de Calfuco, Universidad Austral de Chile, Valdivia, Chile.

[8]Instituto de Fomento Pesquero (IFOP), CTPA-Putemún, Castro, Chile.

[9]Fundación Bariloche and CONICET, San Carlos de Bariloche, Argentina .

[10]Centro Austral de Investigaciones Científicas (CADIC), CONICET, Bernardo Houssay 200, Ushuaia, Argentina.

[11]Centro de Observación Marino para estudios de riesgos del ambiente Costero, Universidad de Valparaíso, Chile.

[12]AGO-GHER, University of Liège, Belgium.

[13]Servicio Hidrográfico y Oceanográfico de la Armada de Chile.

[14]Department of Civil and Environmental Engineering, University of Maine, 5711 Boardman Hall, Orono, ME, USA.

**Correspondence to*: I. Pérez-Santos (ivan.perez@ulagos.cl), https://orcid.org/0000-0002-0184-1122.

Abstract

The dissolved oxygen (DO) levels of coastal ocean waters have decreased over the last decades in part because of the increase in surface and subsurface water temperature caused by climate change, the reduction of ocean ventilation, and the increase in stratification and eutrophication. In addition, biological and human activity in coastal zones, bays, and estuaries has contributed to the acceleration of current oxygen loss. The Patagonian fjord and

channel system is one world region where low DO water (LDOW, 30%–60% oxygen saturation) and hypoxia conditions (<30% oxygen saturation, 2 ml L^{-1} or 89.2 µmol L^{-1}) are observed. An *in-situ* data set of hydrographic and biogeochemical variables (1507 stations), collected from sporadic oceanographic cruises between 1970 and 2021, was used to evaluate the mechanisms involved in the presence of LDOW and hypoxic conditions in northern Patagonian fjords. Results denoted areas with LDOW and hypoxia coinciding with the accumulation of inorganic nutrients and the presence of salty and poor-water Equatorial subsurface water mass. The role of biological activity in oxygen reduction was evident in the dominance of community respiration over gross primary production. This study elucidates the physical and biogeochemical processes contributing to hypoxia and LDOW in the northern Patagonian fjords, highlighting the significance of performing multidisciplinary research and combining observational and modeling work. This approach underscores the importance of a holistic understanding of the subject, encompassing both real-world observations and insights provided by modeling techniques.

1 Introduction

Hypoxic conditions and low dissolved oxygen water (LDOW) have expanded globally over the last decade along coastal waters and oceans (Schmidtko et al., 2017; Breitburg et al., 2018). The origins of the hypoxia and LDOW are attributed to natural and anthropogenic processes. Remineralization of organic matter, weak circulation, extended residence time, and stratification were reported as natural processes (Rabalais et al., 2010; Bianchi et al., 2010). In contrast, water eutrophication was documented as one of the main anthropogenic processes. (Díaz et al., 2001; Conley et al., 2009; Meire et al., 2013). Therefore, for decades, the scientific community has been paying close attention to this issue because of the expected impacts on the survival, abundance, development, growth, reproduction, and behavior of the most important taxonomic groups at different stages of their life cycles, such as mollusks, crustaceans, and fish (Sampaio et al., 2021, Ekau et al., 2010; Batiuk et al., 2009; Vaquer-Sunyer and Duarte, 2008; Breitburg et al., 1997; Díaz and Rosenberg, 1995; Andrewartha and Birch, 1986; Davis, 1975), which could also affect all services provided to humans (Laffoley and Baxter, 2019).

Some examples of the impact of LDOW on biological behaviors are changes in the composition of benthic communities in prolonged periods of DO<4.2 ml L^{-1} (Hoos, 1973), negative impact on the growth and abundance of cod (3.6 ml L^{-1}; 70%), the limit of the distribution of sardine larvae (2.6 ml L^{-1}; 50%), the distribution of jellyfish (1.6 ml L^{-1}; 30%), the decrease of the abundance, swimming capacity and filtration of copepods (0.52 ml L^{-1}; 10%), described by Ekau et al., (2010). Additionally, oxygen deficiency affects the growth rate and feed conversion efficiency, and in some species, even increases the concentration of toxic substances (Davis, 1975). In a Patagonian fjord used for recreational fishing of rainbow trout (*Salmo gairdneri*, values under 50% saturation caused a reduction in swimming speed (Jones, 1971b) and altered respiration and metabolism (Kutty, 1968a). In the case of coho salmon (*Oncorhynchus kisutch*), a commonly farmed species, a growth rate proportional to the oxygen level was observed for saturations between 40% and 80% (Herrmann, 1958), and the hypoxia modulated the transcriptional immunological response (Martinez et al., 2020). Finally, Pérez–Santos et al. (2018) reported habitat reduction of microzooplankton in a Patagonian fjord (Puyuhuapi Fjord) due to the presence of hypoxic conditions at depths below 100 m.

Throughout the world's oceans, there are areas in which the dissolved oxygen (DO) is significantly lower than in well-oxygenated areas (such as <20 µM, ~ 0.4 mg L^{-1}, or 0.31 ml L^{-1}) as shown by Breitburg et al., (2018). These areas are known as oxygen minimum zones (OMZs). OMZs result from organic matter degradation, weak water circulation, long residence times, and weak ventilation (Fuenzalida et al., 2009). The major ocean OMZs are located in the Eastern South Pacific, the Arabian Sea, the Bay of Bengal (Indian Ocean), the West Bering Sea, and the Gulf of Alaska, covering approximately 8% of the total ocean or approximately 30 million km^2 (Paulmier and Ruiz-Pino, 2009; Fuenzalida et al., 2009).

Along the Peru-Chile coastline, the Eastern South Pacific (ESP) Oxygen Minimum Zone (OMZ) extends poleward. As one moves southward, it gradually diminishes in both size and strength until it approaches the Patagonian fjord system (Silva et al., 2009). Recently, Linford et al. (2023) demonstrated poleward transport of hypoxic and LDOW of the Equatorial Subsurface water mass (ESSW) alongside the Patagonian region. As ESSW (originated in the Equatorial region) moves south, it passes throughout the OMZ, carrying oxygen-poor water

(89−134 µM) with high nitrate concentration (20−30 µM) and elevated salinity (34.9) (Silva et al., 2009). Studies of water masses inside Patagonian fjords and channels have detected the presence of ESSW only in the northern region, between 41° S and 45° S. This water mass enters the northern Patagonia region via the Guafo mouth (Figure 1b), a deep channel with a depth of 150−200 m and width of 35 km (Sievers and Silva, 2008; Pérez-Santos et al., 2014; Schneider et al., 2014). ESSW is one of the main causes of hypoxia and LDOW inside Patagonian fjords (e.g., Puyuhuapi Fjord and Jacaf Channel). Nevertheless, these conditions are also found in other areas where sills block the pass of ESSW, e.g., the Reloncaví system (Reloncaví Fjord and Reloncaví Sound), Aysén, Comau, and Quitralco fjords (Figure 1) (Silva and Vargas, 2014; Linford et al., 2023; Díaz et al., 2023).

Regarding other processes favoring hypoxia and LDOW inside Patagonian fjords, Silva (2008) proposed biological processes that include the consumption of DO, such as respiration and the remineralization of organic matter. A high load of organic matter (autochthonous and allochthonous) in the water column and sediments increases DO consumption during microbial community respiration, contributing to the LDOW content in most of the Patagonian fjord headwaters (Castillo et al., 2016) as well as higher community respiration rates than primary production (Montero et al., 2011; Montero et al., 2017a). The main contributor to the increase of allochthonous organic matter is the river supplies, mainly during late winter and early spring, owing to the dominance of ice melt over precipitation during the winter season. The highest river discharges in the region are found in the Puelo, Petrohue, and Cochamo Rivers in the Reloncaví Fjord, the Cisne River in the Puyuhuapi Fjord, and other freshwater contributions from small rivers in the northern Patagonian fjords (Castillo et al., 2016; Schneider et al., 2014). Additionally, weak deep ventilation and long residence times in fjord waters are assumed to promote a reduction in the DO concentration (Schneider et al., 2014; Silva and Vargas, 2014).

The Patagonian fjords ecosystem is under substantial continued economic pressure due to salmon aquaculture and other economic activities (Billi et al., 2022). The northern Patagonian fjords (Figure 1b, 1c) reported half of the national production and a significant number of salmon concessions (Billi et al., 2022). A risk analysis carried out in this region established that the Reloncaví estuarine system, and the Comau, Puyuhuapi, Quitralco, and Cupquelan fjords are regions with an especially elevated level of risk for the development of harmful algal blooms (HABs) and eutrophication events, owing to the nutrients input by the intense aquaculture of salmon (Soto et al., 2021). Nevertheless, environmental studies on salmon farming have shown that this economic activity has a geographically limited impact, because most nutrients are quickly recycled by biological processes in the water column (Soto and Norambuena, 2004).

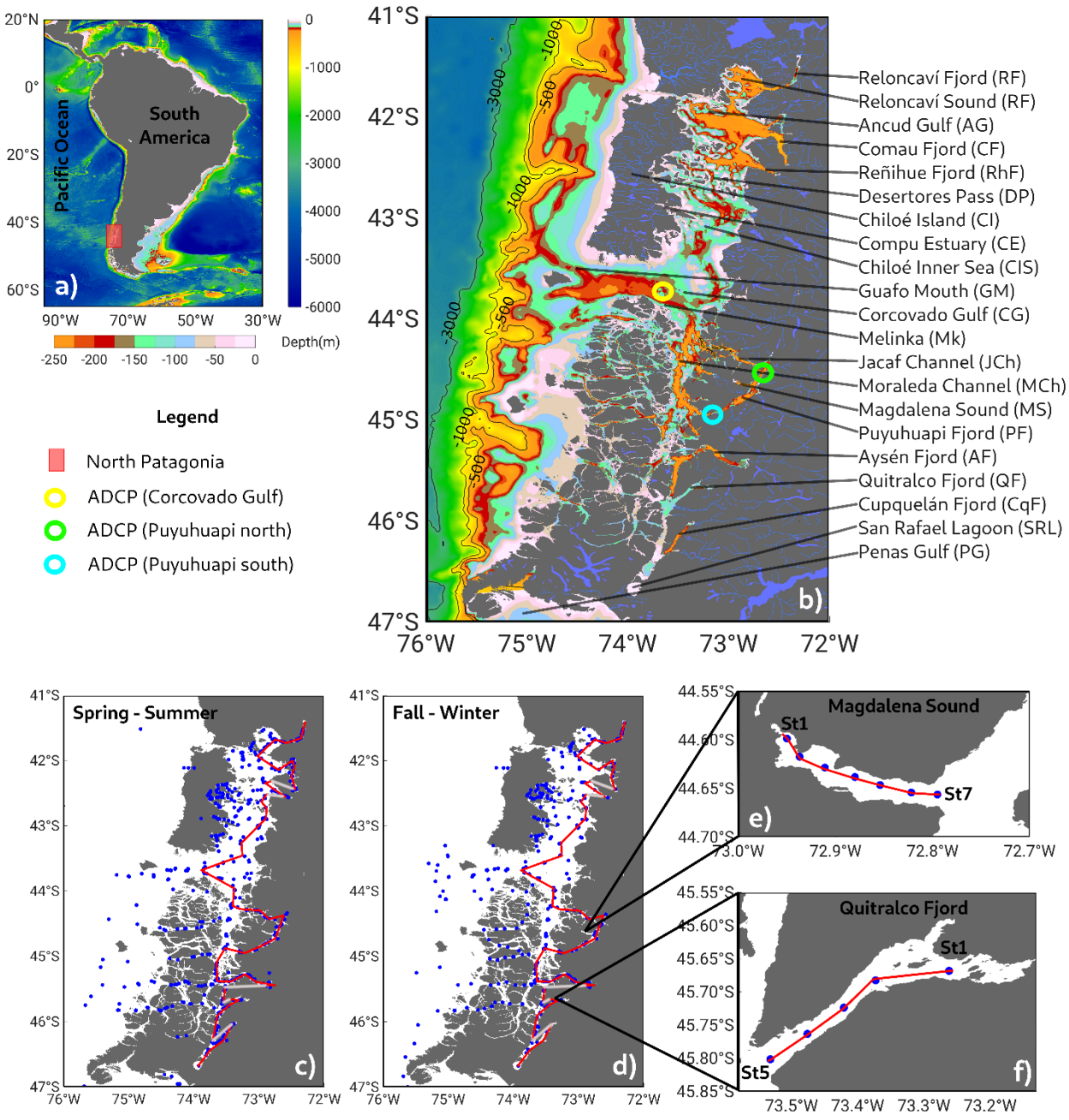

115

Figure 1. (a) Map showing the study area in the (b) northern region of Patagonian fjords. Color bars represent bathymetric features from ETOPO2. (c, d) Sampling stations during the spring-summer and fall-winter seasons. Red lines in (c, d) represent along-fjord transects used to describe vertical features of hydrographic-chemical stations from Figure 2, 4, and 5. Data were collected on sporadic cruises, from 1970–2021 (see Table 1). (e, f) Details of

120 Magdalena Sound and Quitralco Fjord sampling stations. (g, h) High-resolution model domain includes the northern Patagonia inner sea and is denoted as D1_Chiloé, while D2_Aysén covers the southern section. Bathymetry was based on an SHOA (acronym for its Spanish name, Servicio Hidrográfico y Oceanográfico de la Armada de Chile) nautical chart from the Chilean Navy.

Another meaningful impact of salmon production is the increase in allochthonous organic matter load, which, when combined with the high production of autochthonous organic matter by phytoplankton, favors a decrease in DO in the water column and sediments (Quiñones et al., 2019). Salmon farming supplies allochthonous dissolved substrates through the dissolution of organic particles derived from feces and uneaten feed (Wang et al., 2012). This organic material is considered highly degradable (Nimptsch et al., 2015; Montero et al., 2022), promoting enhanced rates of heterotrophic bacterial activity (e.g., bacterial production (BP) and extracellular enzymatic activity (EEA) (Montero et al., 2022).

The main goal of this study was to analyze the processes contributing to hypoxia and LDOW in northern Patagonia, such as ESSW advection, DO consumption during the use of organic matter (community respiration), biogeochemical processes, deep-water ventilation, and residence times of water inside fjords. A combination of the *in-situ* dataset, primary production experiments, and modeling results were used to demonstrate the occurrence of processes promoting low oxygen conditions in the northern Patagonian fjords.

2. Materials and Methods

2.1 Hydrographic and chemical data

A total of 1507 stations were used to describe northern Patagonia's hydrographical and chemical processes; 593 stations were sampled during the fall-winter seasons and 914 during the spring-summer seasons (Table 1). Most temperature and salinity records were obtained using a CTD (Conductivity, Temperature, and Depth profiler) instrument (e.g., SBE19 plus, SBE15, and AML Metrec XL). When SBE CTDs were used, data were processed according to the manufacturer's protocol and software (SBE Data Processing). When using AML CTD, the raw data underwent quality control, eliminating records out of range according to historical CTD data (Pérez-Santos et al., 2014; Pérez-Santos et al., 2021; Linford et al., 2023), after which the data were averaged every 1 m. Additionally, membrane and optical sensors (e.g., SBE 43 and Optode 4831) together with the Winkler method have been used to obtain DO data (Strickland and Parsons, 1968). Experiments were conducted to validate the CTD-DO data with the Winkler method showing satisfactory results and high statistical correlation (R^2 ranging 0.92–0.99, Figure not included).

Figures 1b and 1c show the station positions during fall-winter and spring-summer. The absolute salinity (S_A in gkg^{-1}) and conservative temperature (Θ in °C) were calculated using the Thermodynamic Equation of Seawater 2010 (TEOS-10) (IOC et al., 2010). In TEOS-10, absolute salinity represents the spatial variation in the composition of seawater, considering the different thermodynamic properties and gradients of horizontal density in the open ocean. Conservative temperature is similar to potential temperature but represents the heat content of seawater with greater precision.

A temperature/salinity (TS) diagram was constructed based on the conservative temperature and absolute salinity values, which was used to identify and quantify the water masses in the Patagonian fjords using only the salinity criteria proposed by Sievers (2008) and Sievers and Silva (2008). In Patagonian fjords, the density features of the water column are dominated by the vertical/horizontal distribution of the salinity rather than the water temperature, justifying the use of salinity in the identification of water masses (Aiken 2012; Pérez-Santos et al.,

2014). According to this classification, Estuarine Water (EW, 0-31 g kg^{-1}) originates in the surface layer owing to the water supply from rivers and summer time glacier melting. Below the EW, a Modified Subantarctic Water (MSAAW, salinity 31–33 g kg^{-1}) layer is located from the mixing of the EW with the Subantarctic Water (SAAW, salinity 33–33.8 g kg^{-1}). Finally, an Equatorial Subsurface Water (ESSW) mass represents salinity values higher than 33.8 g kg^{-1}. The ESSW was localized near the bottom of the Puyuhuapi Fjord and Jacaf Channel (Linford et al., 2023).

The long-term seasonal means were calculated using the Data Interpolation Variational Analysis (DIVA) gridding software developed by the University of Liege (http://modb.oce.ulg.ac.be/mediawiki/index.php/DIVA). The DIVA software was used to analyze and interpolate datasets via an optimal interpolation method, which considers the coastline and bathymetry of the study area; the calculations were executed on a finite element mesh adapted to the study area domains (Troupin et al., 2010). Additionally, the DIVA results were graphically displayed using the Ocean Data View software (https://odv.awi.de).

Table 1. Oceanographic campaigns carried out in Patagonian fjords and channels.

Expeditions	Date	Season	Stations	Measurements
HUDSON	06/03-01/04, 1970	Summer	112	(Temperature, Salinity) * + O2(bottle-Winkler) + Nutrients (PO4, NO3, Si; bottle)
CIMAR-01	18/10-04/11, 1995	Spring	99	CTD + O2(bottle-Winkler) + Nutrients (PO4, NO3, NO2, Si; bottle) + pH(bottle)
CIMAR-04-I	28/09-09/10, 1998	Spring	31	CTD + O2(bottle-Winkler) + Nutrients (PO4, NO3, Si; bottle)
CIMAR-07-I	07-21/07/2001	Winter	49	CTD + O2(bottle-Winkler)
CIMAR-07-II	13-25/11/2001	Spring	51	CTD + O2(bottle-Winkler) + Nutrients (PO4, NO3, Si; bottle)
CIMAR-08-I	06-20/07/2002	Winter	51	CTD + O2(bottle-Winkler) + Nutrients (PO4, NO3, Si; bottle)
CIMAR-08-II	16-24/11/2002	Spring	39	CTD + O2(bottle-Winkler) + Nutrients (PO4, NO3, Si; bottle)
CIMAR-09-I	09-23/08/2003	Winter	58	CTD + O2(bottle-Winkler) + Nutrients (PO4, NO3, Si; bottle)
CIMAR-09-II	07-20/11/2003	Spring	55	CTD + O2(bottle-Winkler) + Nutrients (PO4, NO3, Si; bottle)
CIMAR-10-I	26/06-31/08, 2004	Winter	49	CTD + O2(bottle-Winkler) + Nutrients (PO4, NO3, Si; bottle)
CIMAR-10-II	12-23/11/2004	Spring	63	CTD + O2(bottle-Winkler) + Nutrients (PO4, NO3, Si; bottle)
CIMAR-11-I	18-25/07/2005	Winter	78	CTD + O2(bottle-Winkler) + Nutrients (PO4, NO3, Si; bottle)
CIMAR-11-II	11-21/11/2005	Spring	80	CTD + O2(bottle-Winkler) + Nutrients (PO4, NO3, Si; bottle)
CIMAR-12-I	10-19/07/2006	Winter	32	CTD + O2(bottle-Winkler) +Nutrients (PO4, NO3, Si; bottle)
CIMAR-12-II	04-12/11/2006	Spring	40	CTD + O2(bottle-Winkler) + Nutrients (PO4, NO3, Si; bottle)
CIMAR-13-I	27/07-07/08, 2007	Winter	42	CTD + O2(bottle-Winkler) + Nutrients (PO4, NO3, Si; bottle)
CIMAR-13-II	02-12/11/2007	Spring	46	CTD + O2(bottle-Winkler) + Nutrients (PO4, NO3, Si; bottle)
CIMAR-17	17/10-14/11, 2011	Spring	195	CTD + O2(bottle-Winkler) + Nutrients (PO4, NO3, Si; bottle)
CIMAR-18	01/06-04/07, 2012	Fall-Winter	98	CTD + O2(bottle-Winkler) + Nutrients (PO4, NO3, Si; bottle)
CIMAR-19	04-16/07/2013	Winter	70	CTD + O2(bottle-Winkler) + Nutrients (PO4, NO3, Si; bottle)
CHEPU-IFOP	05-17/08/2017	Winter	22	CTD + O2(optic)
CIMAR-24	26/09-16/10, 2018	Spring	37	CTD + O2(bottle-Winkler) + Nutrients (NO3; bottle)
CHEPU-MR-I	06-08/06/2018	Fall	12	CTD + O2(optic)
CHEPU-MR-II	11/10/2018	Spring	2	CTD + O2(optic)

PN-I (IFOP)	13-25/11/2020	Spring	32	CTD + O2(optic) + Nutrients (PO4, NO3, NO2, Si; bottle) + pH, Tur, Fluor (optic)
PN-II (IFOP)	24/02-04/03, 2021	Summer	32	CTD + O2(optic) + Nutrients (PO4, NO3, NO2, Si; bottle) + pH, Chl-a, Tur, Fluor (optic)
PN-III (IFOP)	28/07-10/08, 2021	Winter	32	CTD + O2(optic) + Nutrients (PO4, NO3, NO2, Si; bottle) + pH, Chl-a, Tur, Fluor (optic)
				593 Fall-Winter + 914 Spring-Summer = 1507 stations

*Temperature and salinity were measured with a reversing thermometer and inductive salinometer respectively.

2.2 Primary production, community respiration, bacterial production, and phytoplankton community.

During the spring-summer period of 2020–2021 and summer of 2022, nine *in situ* experiments were conducted to measure gross primary production (GPP) and community respiration (CR) in some fjords of northern Patagonia (Table 2). Water samples were obtained from three depths (2, 10, and 20 m depth) at each sampling station. GPP and CR rates were estimated from changes in DO concentrations observed during *in situ* incubation of light and dark bottles (Strickland, 1960). Water from the Niskin bottles was transferred into 125 mL (nominal volume) borosilicate bottles (gravimetrically calibrated) using a silicone tube. Five time-zero bottles, five light bottles, and five dark bottles were used at each incubation depth. Water samples were collected at dawn and incubated throughout the entire light period (approximately ~8-9 h). Time-zero bottles were fixed at the beginning of each experiment, whereas the light and dark incubation bottles were attached to the surface-tethered mooring system. The samples were incubated at the depths from which they were collected. Additionally, we presented GPP and CR values from February 2009 in Figure 9, which have been previously published by Montero et al. (2011).

Dissolved oxygen concentrations were determined according to the Winkler method (Strickland and Parsons, 1968), using an automatic Metrohom burette (Dosimat plus 865) and automatic end-point detection (AULOX Measurement System). Daily GPP and CR rates were calculated as follows: GPP = (mean [O_2] light bottles – mean [O_2] dark bottles); CR = (mean [O_2] time zero bottles – mean [O_2] dark bottles). The GPP and CR values were converted from oxygen to carbon units using a conservative photosynthetic quotient of 1.25 (Williams and Robertson, 1991) and a respiratory quotient of 1.

A total of five bacterial production (BP) experiments were performed during the same period as mentioned above (Table 2). Experiments were conducted using the same water samples collected for the *in situ* GPP and CR incubation experiments. The BP estimates were based on the incorporation of leucine into proteins using the microcentrifugation method (Smith and Azam, 1992). Briefly, a blank and three samples (1.5 mL) were taken from each sampling depth and incubated with L-[3,4,5-^{3}H]-leucine (123.8 Ci mmol^{-1}, 40 nM final concentration) in the dark for 1 h. After incubation, samples were extracted with 100% trichloroacetic acid (TCA), rinsed with 5% TCA, and centrifuged at 13500 rpm twice for 15 min before removal of the supernatant. Liquid scintillation cocktail Ecoscint (1 mL) (National Diagnostic) was added to each sample. The samples were counted for dpm using a Packard (Mod. 1600 TR) liquid scintillation counter. Discrete depth estimates of the GPP, CR, and BS rates were integrated to 20 m using the trapezoidal method.

For analyses of the phytoplankton community, water samples were collected from four discrete depths (2, 4, 10, and 20 m) using a 5 L Niskin bottle. Samples were stored in 120 mL clear plastic bottles and preserved in 1% Lugol's iodine solution (alkaline). From each sample, a 10 mL subsample was placed in a sedimentation chamber

and allowed to settle for 12 h (Utermöhl, 1958) prior to identification at 40× and 100× under an inverted microscope (Carl Zeiss, Axio Observer A.1). Finally, taxonomic descriptions from Tomas (1997) were used to identify phytoplankton composition.

Table 2. Gross primary production (GPP), community respiration (CR), and bacterial secondary production (BSP) from in situ experiments in northern Patagonian fjords and channels.

Fjord region	Date (mm-dd-yyyy)	Season	Measurements (g C $m^{-2}d^{-1}$)			
			GPP	CR	BSP	GPP:CR
*Reloncaví	02/27/2009	Summer	3.83	3.31	-	1.16
Compu	10/03/2020	Spring	1.22	0.92	0.06	1.32
Quitralco	11/17/2020	Spring	1.41	2.66	0.05	0.53
Camou	12/12/2020	Spring	0.12	1.67	0.15	0.07
Puyuhuapi	01/21/2020	Summer	1.89	6.64	0.25	0.28
Reloncaví	01/14/2021	Summer	2.60	1.90	0.58	1.37
Compu	03/19/2022	Summer	1.25	0.76	-	1.64
Quitralco	02/28/2022	Summer	0.73	1.71	-	0.42
Camou	03/16/2022	Summer	0.56	1.12	-	0.50
Puyuhuapi	01/20/2022	Summer	2.18	2.55	-	0.85

*Data were taken from Montero et al. (2011).

2.3 Biogeochemical variables and analysis

Biogeochemical data were collected in November 2020 (Expedition PN-I IFOP, Table 1). The water samples were obtained by filtering seawater collected (1−2 L) using a 25-mm diameter, GF/F filter pre-combusted with a 0.7µm pore diameter. Suspended particulate matter (SPM, µg L^{-1}), was determined by gravimetry using the weight difference between the dried filter and the same filter before filtration (Grasshoff et al., 2009). Particulate organic carbon (POC, µmol L^{-1}), total nitrogen (TN, µmol L^{-1}), stables carbon ($\delta^{13}C$, ‰) and nitrogen ($\delta^{15}N$, ‰) isotopes were obtained following the method described by Verardo et al., (1990), with modifications by Barrera et al., (2017) and Díaz et al., (2023), and measured at the Stable Isotope Facility at the Pontifical Catholic University of Chile by using an elemental analyzer (EA Flash 2000 Thermo Finnigan), interfaced to a continuous flow isotope ratio mass spectrometer (IRMS Delta V Advantage).

The stable carbon isotope composition of organic carbon ($\delta^{13}C$) can vary depending on its origin, with values ranging from −23 to −19‰ for carbon sources such as marine phytoplankton (Fry and Sherr, 1989; Harmelin-Vivien et al., 2008) and values closer to those of terrestrial organic matter (−30 to −26‰) for other sources (Fry and Sherr, 1989).By analyzing the carbon isotopic composition of organic carbon, it is possible to differentiate carbon between different sources and estimate their contributions. We calculated the relative importance of allochthonous and autochthonous organic matter with two-source endmember mixing models (Bianchi, 2007). The importance of autochthonous marine and allochthonous terrestrial fractions was calculated based on the following equation:

$$\%POC_{allo} = \frac{(\delta^{13}C_s - \delta^{13}C_m)}{(\delta^{13}C_t - \delta^{13}C_m)} 100\%$$

where $\delta^{13}C_s$ is the isotopic composition of a sample, $\delta^{13}C_m$ is the marine endmember from more oceanic stations (-13.447 ‰), and $\delta^{13}C_t$ terrestrial is the riverine/lake endmember values for POC (-42.933 ‰) as proposed for this

area by González et al., (2019). The resulting $\%POC_{allo}$, represents the relative contribution of allochthonous (terrestrial) organic carbon to the overall organic carbon pool. Higher values indicate a more significant influence of terrestrial organic carbon, while lower values suggest a higher proportion of autochthonous (marine) organic carbon (González et al., 2019). The carbon: nitrogen ratio was also calculated as a proxy for the organic matter pool (Barrera et al., 2017).

Dissolved inorganic nutrients (NO_3^-, NO_2^-, PO_4^{3-}, and $Si(OH)_4$) were analyzed from 15 mL seawater samples, stored at -20 ºC in HDPE bottles, using a Seal AA3 Autoanalyzer according to the methodology described by Grasshoff et al., (1983) and standard methods for seawater analysis (Kattner and Becker, 1991). Chromophoric Dissolved Organic Matter (CDOM) plays a crucial role in understanding the optical properties and biogeochemical processes in aquatic ecosystems (Stedmon and Nelson, 2015). It is an important component of dissolved organic matter (DOM) that absorbs light in the visible spectrum (ultraviolet and blue wavelengths) and fluoresces at longer wavelengths (Stedmon and Nelson, 2015). CDOM was determined by fluorometry using quinine sulfate dihydrate (μgL^{-1} QSU) diluted in 0.1 N sulfuric acid at a specific wavelength (Ex/Em = 350/450 nm) as standard in a Trilogy Turner Design fluorometer and CDOM module (Kim et al., 2018).

2.4 Satellite images

Sentinel-2 level 1 images were downloaded from the Copernicus Open Access Hub (https://scihub.copernicus.eu/) for specific dates and regions, as shown in Table 3. The chosen dates correspond to periods of high discharge of freshwater from the continent. Using ACOLITE v 20220222.0 (https://odnature.naturalsciences.be/remsem/software-and-data/acolite, Vanhellemont and Rudick, 2018), we calculated the satellite suspended particulate matter (SSPM) following Nechad et al. (2016). These data have a spatial resolution of 10 m and allow the resolution of the small-scale distribution of SSPM within the narrow channels and fjords of the region.

Table 3. Dates and regions of the Sentinel-2 datasets analyzed.

Date	Region
17 March 2017	Puyuhuapi Fjord
09 May 2017	Reloncaví Sound and Fjord
06 April 2018	Comau Fjord
09 June 2022	Quitralco Fjord

2.5 Marine current registered with ADCP

In the study region, three mooring systems were deployed in the Corcovado Gulf and Puyuhuapi Fjord. In each mooring, a Teledyne RD Instruments (TRDI) and a WorkHorse−300 kHz Acoustic Doppler Current Profiler (ADCP) were installed with the transducers facing downward. The instruments were configured with 1-m cell size and 1 h ensembles. The moorings covered the period from January to December 2016, with the ADCP sensors moored between 40 and 100 m. The ADCP provides the current magnitude and direction (in Earth coordinates); thus, the current vector is decomposed into zonal (u) and meridional (v) components. The basic and standard protocol of quality control was applied to identify outliers and low-quality data following the methodology

suggested by TRDI. To obtain the mean pattern of the zonal and meridional components of the currents, they were filtered using a low-pass cosine-Lanzcos filter of 121 weight and 40 h half-power.

The currents were rotated following the main axis of the Guafo channel and Puyuhuapi Fjord (Figure 1), thus implying that in Guafo, currents were rotated 14º south of east whereas in Puyuhuapi south currents were rotated 36º north of the east and in Puyuhuapi north the axis was rotated 22º east of north. Following those rotations, the contours of the time series of the along-channel/fjord components are shown in Figure 11.

2.6 Circulation model

To enhance our understanding of the DO dynamics' and physical factors, we utilized the MIKE 3 FM hydrodynamic model. This model employs the finite volume method to solve continuity, momentum, temperature, and salinity transport equations (DHI, 2019). This study focused on two high-resolution model domains: D1_Chiloé (41.3° S to 43.7° S) and D2_Aysén (43.6°S to 46.8° S) (Figures S1a, S1b).

The D1_Chiloe and D2_Aysen models are part of the 'CHONOS' Initiative (Reche et al. 2021), available at chonos.ifop.cl. This platform offers an open-access oceanographic database, primarily tailored for environmental applications. Led by the Instituto de Fomento Pesquero (IFOP) and supported by the Undersecretariat for Fisheries and Aquaculture of the Chilean Government, this system guides decisions concerning aquaculture in southern Chile. Moreover, this oceanographic database, grounded in the D1 and D2 domains, has been used in studies on harmful algal blooms (Mardones et al. 2021; Diaz et al., 2021), larval fish dispersion (Landaeta, 2023), and overarching marine circulation dynamics (Soto Riquelme et al. 2023; Perez Santo et al. 2019). The modeling process was conducted over six years, from 2016 to 2021. Owing to computational constraints, the development began with the D1_Chiloe domain, subsequently followed by D2_Aysen. Both domains employed a hydrostatic variant of the MIKE 3 model. Vertical discretization was implemented using hybrid coordinates, combining sigma and z-level systems. The bathymetry was sourced from the nautical chart soundings provided by the Chilean Navy (www.shoa.cl).

For atmospheric forcing, we used the Weather Research and Forecasting (WRF) model from the 'CHONOS' Initiative. This version provides a refined 3km spatial resolution, tailored for the complex topography of the fjords. Its efficacy was previously described by Soto-Riquelme et al. (2023), who specifically evaluated its performance near the Guafo Mouth, finding significant correlations with local meteorological stations, particulary in atmospheric pressure (R=0.99) and wind (R=0.87).

Freshwater sources were identified through the FLOW-IFOP hydrological model, which employs precipitation and temperature series data from the CR2MET gridded product (http://www.cr2.cl/datos-productos-grillados/). Using these data, characterized by a spatial resolution of 5 × 5 km, enables the simulation of runoff and the calculation of daily discharge series. Based on FLOW-IFOP estimates, the average annual freshwater discharge entering the D1_Chiloé domain during 2016–2021 was approximately 2545 $m^3 s^{-1}$. Conversely, for the D2_Aysén domain, it was approximately 3126 $m^3 s^{-1}$. The performance of the FLOW-IFOP model at the gauged river stations of the Chilean Water Authority can be accessed at http://chonos.ifop.cl/flow/ and in the Supplementary Material.

Water levels at the open boundary were established using harmonic analysis (Pawlowicz et al., 2002), based on data from a regional barotropic model (Pinilla et al., 2012). Temperature and salinity boundary conditions were compiled from CTD profiles, collected during the CIMAR FIORDOS oceanographic cruises (Guzman and Silva 2002; Silva and Guerra 2004; Valdenegro and Silva 2003; Carrasco and Silva 2010). Finally, boundary flow data were set to zero, ensuring an internal balance of current dynamics within the model domain both temporally and spatially. For an in-depth understanding of the configuration and model validation, kindly refer to the Supplementary Material (Figures S1–S8).

2.7 Flushing time calculation

The MIKE 3 FM hydrodynamic model data were used to calculate the flushing time via a conservative tracer. According to Takeoka (1984) and Monsen et al. (2002), flushing time is defined as the time required for the total mass of a material within a specific area such as a fjord, sound, or bay to be reduced by a factor of e^{-1} (approximately 37%) (Prandle, 1984). The interior and exterior of the area were assigned initial concentration values of 1 and 0, respectively. Throughtoutthe simulation, the original water mass of the basin was incrementally replaced with inputs from open boundaries and rivers. This variable symbolizes the proportion of original water in each element within the area of interest at a given time, facilitating the identification of less flushed areas within the modeled basins (Andrejev et al., 2004). The final values were derived from a temporal average from 2016 to 2021, and a vertical average was calculated from 50 m to the bottom, which represents the area that typically displays the lowest oxygen values. In the present study, the flushing time was implemented in the Ecolab module of the MIKE 3 FM for every fjord within D1_Chiloé and D2_Aysén.

3 Results

3.1. Long-term annual mean of hydrographic-chemical parameters

The long-term annual means include all data sets presented in Figures 2a and 2b (location and detailed information in Figures 1c, d and Table 1). This section scrutinizes the behavior of conservative temperature, absolute salinity, DO, and inorganic nutrients. The long-term seasonal mean of conservative temperature (CT) denoted warmer water in the northern region (41.5°–43° S) during both seasons, between the Desertores Pass and the Reloncaví Fjord (Figure 2c-d)**.** In contrast, cold waters were observed in the deep layer of the Puyuhuapi Fjord and Jacaf Channel, and the coldest water was registered in San Rafael Lagoon. This location also had the lowest absolute salinity (S_A=15–21 gkg^{-1}), indicating the presence of EW owing to the contribution of the ice melting from the San Rafael Lagoon and river discharges (Figure 2e-f). In this area, EW moved from south to north and mixed with the SAAW, contributing to the origin of the MSAAW, as was observed in the vertical-horizontal salinity distribution. Moreover, EW was also observed in the northern domain of the study area, especially at the surface layer in the Reloncaví system and the Comau and Reñihue fjords, contributing to the formation of the MSAAW. In this region, the origin of EW was mainly attributed to the freshwater supply from river discharge. Therefore, we identified two different sources of EW that led to the formation of the MSAAW: 1) The combination of ice melting from the San Rafael Lagoon with river discharge in the southern region and 2) the freshwater supply by river

discharge in the northern region. Both sources contributed to the difference in conservative temperature observed in the MSAAW.

Finally, ESSW enters the deep layer of the Guafo mouth, crosses the Corcovado Gulf, and ends its travel at the deep layers of the Puyuhuapi Fjord and Jacaf Channel. During the fall-winter season, a slight reduction in ESSW distribution was observed (Figure 2e–f). In the area contained by the ESSW, low DO (LDOW) and hypoxic waters were observed, but LDOW was registered at Reloncaví Fjord, where ESSW was not observed (Figure 2g–h).

In general, the Chiloé Inner Sea showed a homogenized water column, during the fall-winter seasons, in which high DO values (267−312 μmol L^{-1}) and oversaturated waters (DO Saturation > 100%) were registered. In addition, high DO records were measured in the San Rafael Lagoon, between the Aysén and Puyuhuapi fjords, and in the Corcovado Gulf (Figure 2g–h). Furthermore, a larger area with hypoxic conditions and LDOW was recorded during the spring-summer seasons (Figure 2g-2h) compared to the autumn-winter period. (Figure 2g–2h).

The quantification of water masses through a TS diagram (Figure 3) highlights the dominance of the MSAAW, with proportions of 60.96% and 54.67% during the spring-summer and fall-winter seasons, respectively. Following closely, the SAAW was the second dominant water mass, with proportions of 15.25% and 22.64%. The EW came next, and finally, the ESSW displayed the smallest proportion, with values of 10.77% and 11.15%. It is worth noting that ESSW was characterized by cold, salty, and poor DO content in comparison to the EW, MSAAW, and SAAW, as detailed in Table 4.

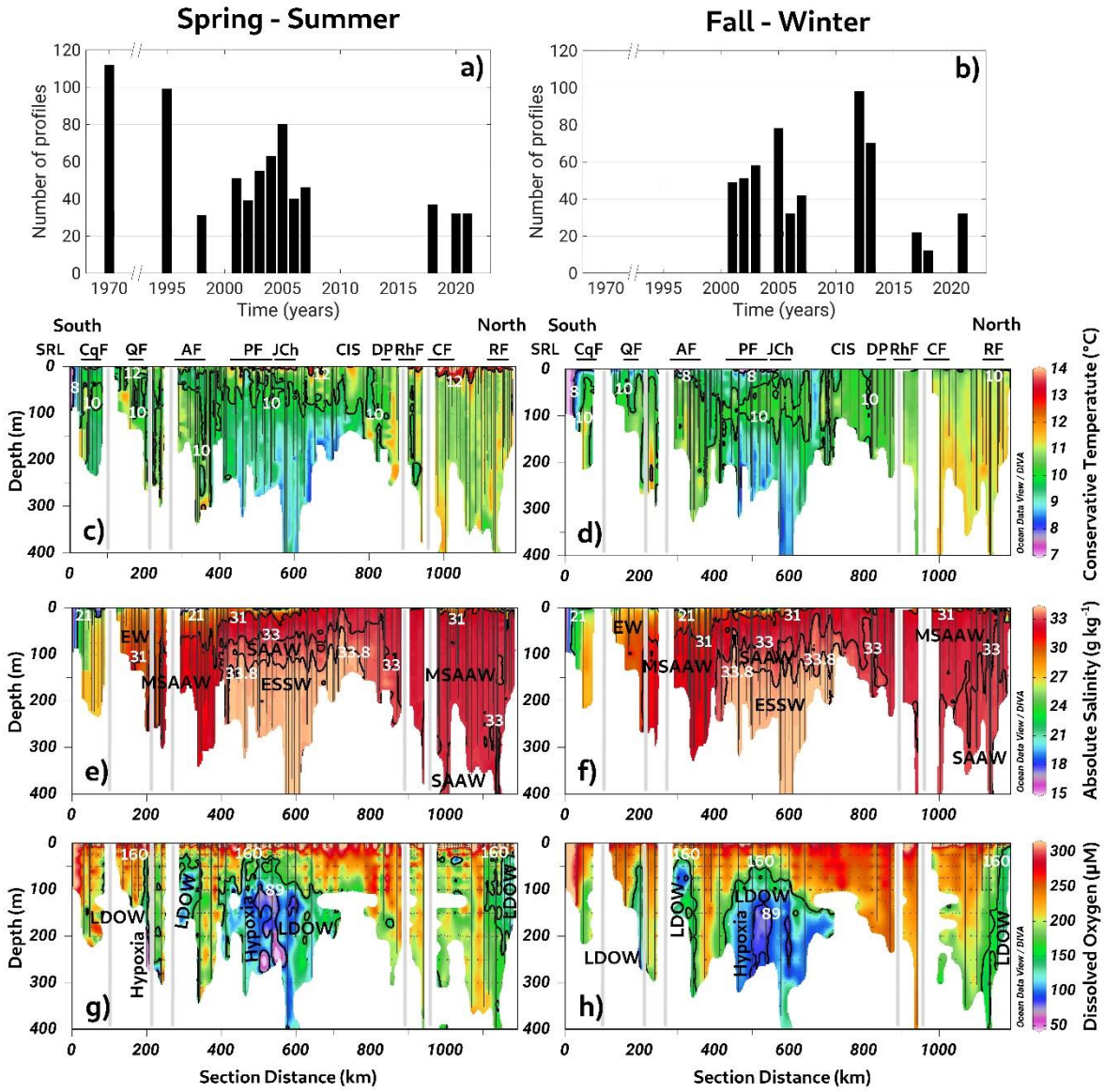

Figure 2. (a, b) Time series of conductivity, temperature, and depth (CTD) profiles used to compute seasonal averages. Long-term seasonal means of (a–b) conservative temperature, (c–d) absolute salinity, and (e–f) dissolved oxygen collected along a vertical section in the northern Patagonian fjord during the fall-winter and spring-summer seasons. See Figure 1b for the acronymous in (c) and (d).

Table 4. Statistical characteristics of the water masses identified in the northern Patagonian fjords.

Salinity criteria (Sievers and Silva, 2008)		Spring-Summer Campaigns				Fall-Winter Campaigns			
Water masses	Salinity range (g kg^{-1})	Water masses (%)	CT (°C) Mean Std[a]	S_A (g kg^{-1}) Mean Std	DO (µmol L^{-1}) Mean-Std	Water masses (%)	CT (°C) Mean Std	S_A (g kg^{-1}) Mean Std	DO (µmol L^{-1}) Mean-Std

EW	0–31	12.64	10.29 ±1.1	27.92 ±4.7	245.25 ±65.8	11.92	9.70 ±0.8	28.75 ±3.4	238.02 ±56.8
MSAAW	31–33	60.96	10.64 ±0.5	32.44 ±0.5	197.11 ±46.2	54.67	10.55 ±0.6	32.34 ±0.5	231.82 ±37.6
SAAW	33–33.8	15.25	10.49 ±0.6	33.25 ±0.2	196.03 ±41.9	22.64	10.85 ±0.6	33.19 ±0.2	208.34 ±46.1
ESSW	33.8>	11.15	9.12 ±0.4	34.11 ±0.1	109.57 ±32.6	10.77	9.27 ±0.5	34.13 ±0.1	114.77 ±36.0

[a]Std: standard deviation.

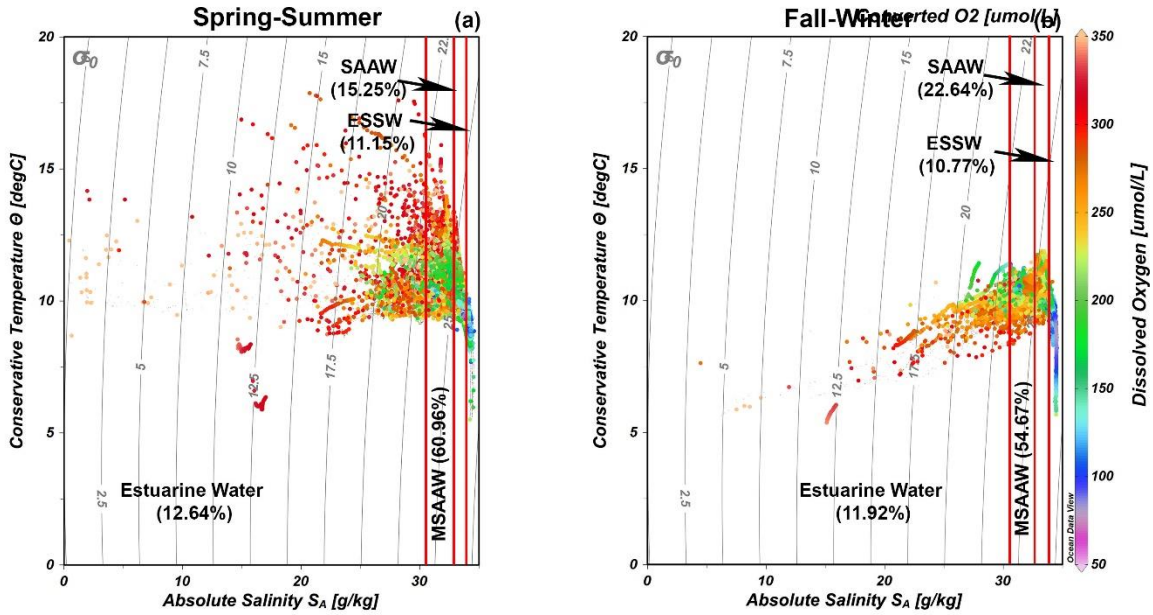

Figure 3. Temperature/salinity (TS) diagram with dissolved oxygen records showing the representation of water masses identified during (a) spring-summer and (b) fall-winter seasons in the northern Patagonian fjords. The dataset utilized in the TS diagram is described in Table 1.

As shown in Fig. 2, the Puyuhuapi Fjord and Jacaf Channel were regions where high-salinity and hypoxic-LDOW waters were registered. In addition, a high concentration of inorganic nutrients was observed in the subsurface layer at depths greater than 50 m (Figure 4). In the Puyuhuapi Fjord and the Jacaf Channel, between 100−300 m depth, nitrate (Figure 4a), phosphate (Figure 4c), and silicic acid (Figure 4e) range from 25–30 µM, 2–3 µM, and 30–50 µM, respectively. A second area with high inorganic nutrients was detected in the Reloncaví system, in which the highest absolute values of surface silicic acid were registered during the fall-winter season (e.g., 210 µM). Comparing seasonal concentrations, the fall-winter season showed the highest abundance in the water column. However, the absolute maximum nitrate (Figure 4b), phosphate (Figure 4d), and silicic acid (Figure 4f) values were recorded in the subsurface layer during the spring and summer seasons.

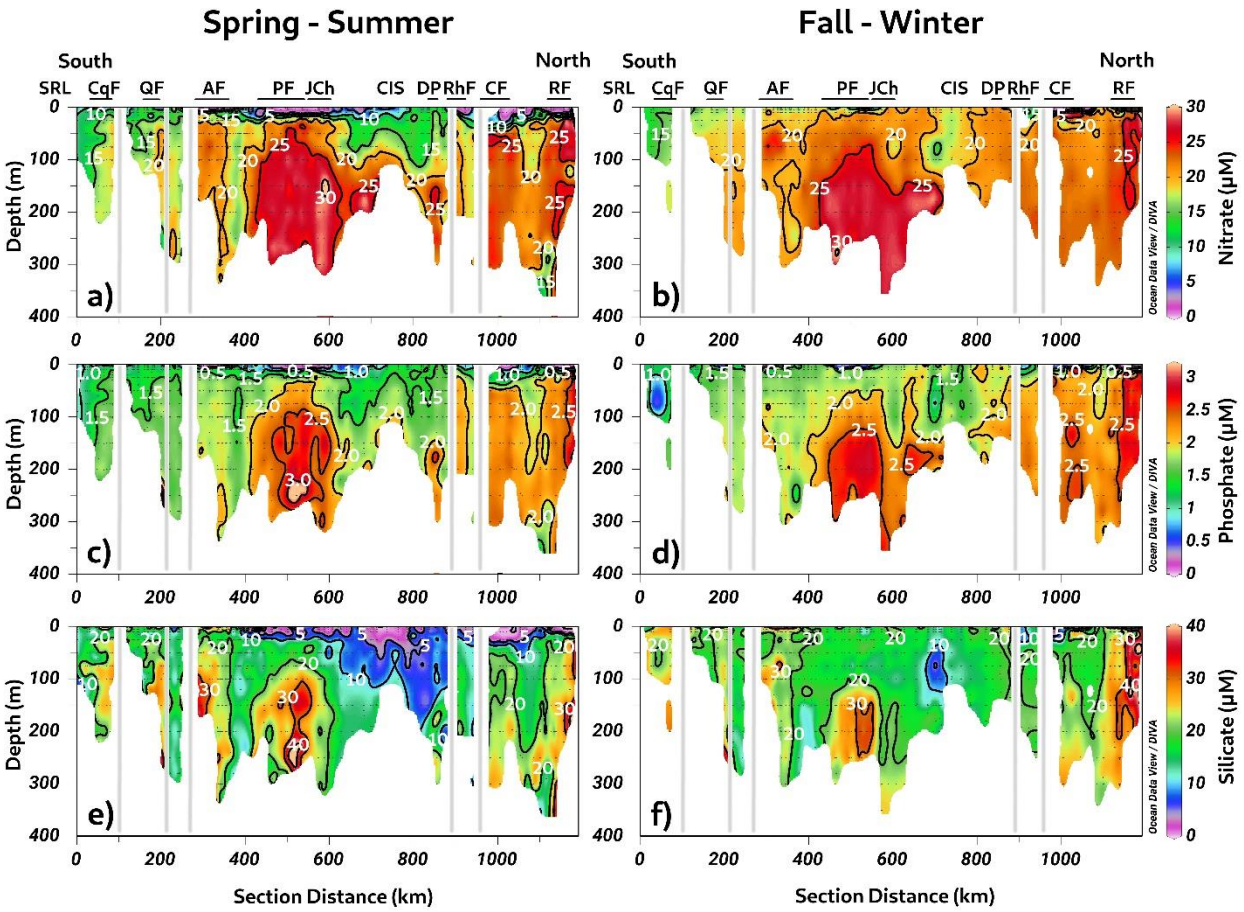

Figure 4. Long-term seasonal mean of inorganic nutrients. (a, b) Nitrate, (c, d) phosphate, and (e-f) silicate collected along a vertical section in the northern Patagonian fjord system during fall-winter and spring-summer seasons.

The calculation of the Brunt-Väisälä frequency (BVF), a variable used to identify mixed/stratified regions, evidenced a permanent mixing of the water column in the Chiloé inner sea (BVF<10 cycl h^{-1}) (Figure 5a–b). Furthermore, the homogenization of physical (e.g., conservative temperature and absolute salinity) and chemical (e.g., DO oxygen and inorganic nutrients) variables was observed in these regions. In contrast, stratified water (between 2 and 10 m depth) was detected during spring-summer inside the fjords, e.g., Cupquelan, Quitralco, Aysén, Puyuhuapi, Comau, and Reloncaví, showing values over BVF>50 cycl h^{-1} that coincided with the lower salinity (Figure 5a). The main drivers of the stratification in the northern Patagonian fjords depended on the freshwater supply by rivers and precipitations affecting the surface. The highest river flow relies on the melting of ice that occurs during the spring, but during the fall and winter, rivers flow is also increased due to the precipitation regime. Additionally, stratification was enhanced in summer because of the increase in solar radiation, making the spring-summer season the period where the absolute maximum stratification was registered (e.g., ~100 cycl h^{-1}) (Figure 5a).

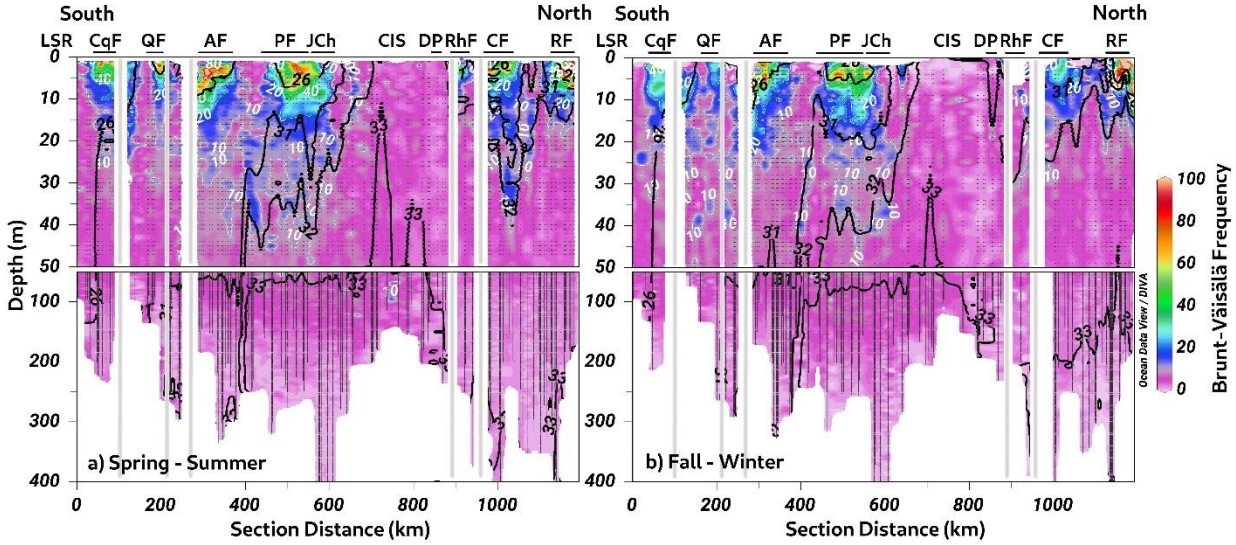

Figure 5. The long-term seasonal mean of Brunt-Väisälä frequency along a vertical section in the northern Patagonian fjords during the (a) spring-summer and (b) fall-winter seasons. The white and black contour lines denote the Brunt-Väisälä and absolute salinity values.

3.2. DO and chlorophyll-a features from sporadic oceanographic cruises.

The analysis of hypoxia and LDOW conditions in the northern Patagonian fjord system highlighted the presence of two areas with water bodies with these characteristics: the Puyuhuapi-Jacaf and Reloncaví regions. Moreover, Magdalena Sound (44.6° S, 72.9° W), located between the Puyuhuapi Fjord and the Jacaf Channel (Figure 1), showed the shallowest hypoxia over the entire northern Patagonian fjords. At this location, a 30% DO saturation isoline was observed at a depth of 70 m, with the LDOW reaching a depth of approximately 20 m (Figure 6a–c). Additionally, the lowest DO values of the northern Patagonian fjord system (9.36 µmol L^{-1} and 1.6% oxygen saturation) were recorded at the deepest layer (~200 m) of the Quitralco Fjord (45.7° S, 73.3° W) (Figure 6d–f).

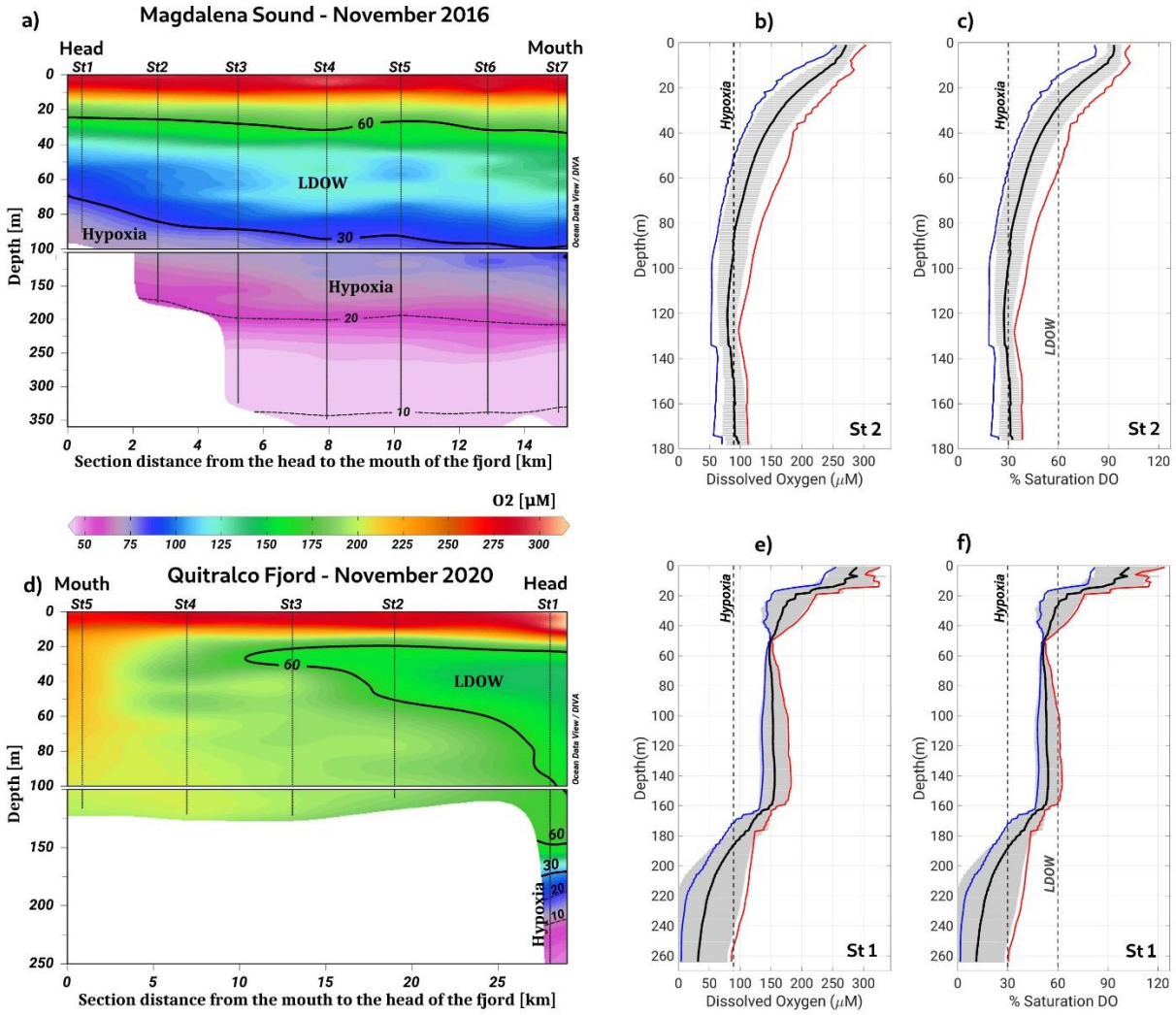

425

Figure 6. Vertical section of dissolved oxygen along (a-c) Magdalena Sound and (d-f) Quitralco Fjord during November 2016 and November 2020, respectively. In (b, c, e, f), red, black, and blue lines represent the absolute maximum, average, and minimum values of DO, respectively. Grey horizontal lines show the standard deviations calculated using 16 profiles for Magdalena Sound and 3 profiles for the Quitralco Fjord.

430

The chlorophyll-a (Chl-a) data collected during two oceanographic campaigns (Figure 7a) denoted high concentrations of Chl-a in the Reloncaví Fjord, the Puyuhuapi Fjord, and the Jacaf Channel (Figure 7b, 7c) where LDOW and hypoxia conditions were registered. The Chl-a values observed during the winter season in the Reloncaví Fjord were exceptionally high (32.8 mg m^{-3}), which discussed in Section 4. Regardless, in general, the
435 winter season of August 2021 showed a lack of Chl-a in the southern part of the study area (Figure 7c). The vertical distribution of the Chl-a data described earlier was obtained through a statistical analysis between the fluorescence data from casts CTD (every 1-m depth) and the in-situ Chl-a samples from discrete levels (i.e., 0, 5, 10, 15, 25, and 50 m) (Figure 7d–e).

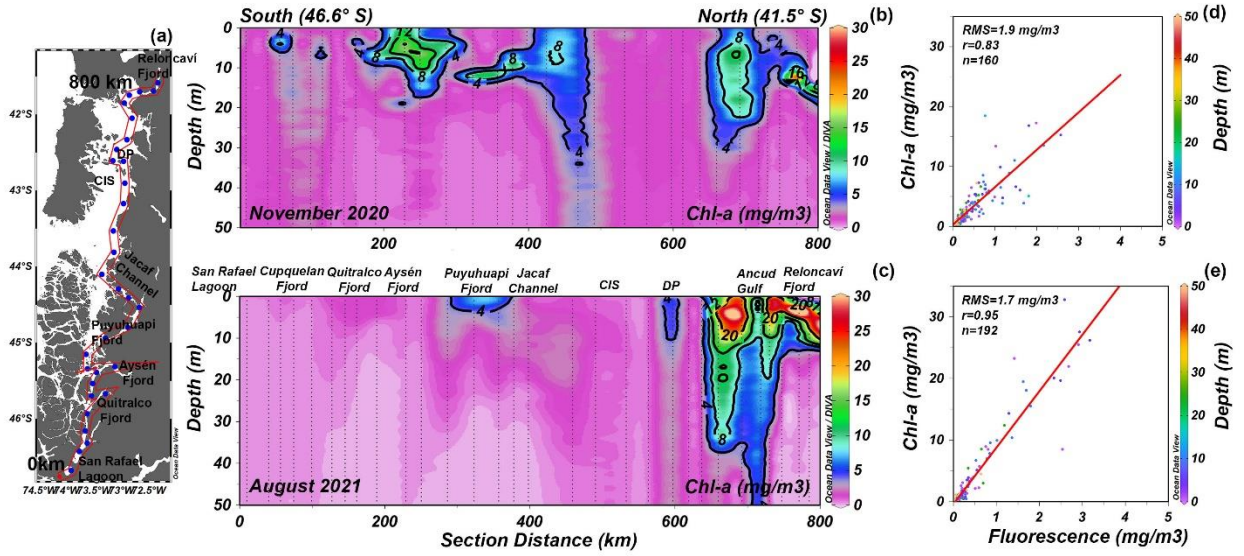

Figure 7. (a) Distribution map of the stations. Vertical distribution of chlorophyll-a (Chl-a) during (b) November 2020 and (c) August 2021 in the northern Patagonian fjords. (d and e) Statistical relationship between the fluorescence data from CTD and in-situ Chl-a samples. In (d and e) RMS is the root mean square, n is the number of data points used to obtain the R-values, and red lines represent the lineal tendency fit in (b and c) CIS is Chiloé Inner Sea and DP is Desertores Pass.

3.3. Rates of primary production, community respiration, and bacterial production

The GPP and CR estimates obtained in our sampling agreed well with measurements reported in previous studies for the Patagonian fjords during the productive period (Iriarte et al., 2007; Montero et al., 2011; Montero et al., 2017a). The GPP and CR rates showed a weak coupling, with most experiments indicating that less oxygen is produced than consumed (Figure 8a). Thus, most fjords exhibited heterotrophic metabolism (GPP:CR <1) in the surface layer (0–20 m) during the study period (Figure 8b). The highest rates of GPP in terms of oxygen (18.6 to 41.02 mmol O_2 m^{-3} d^{-1}) were mainly recorded in the upper 5 m of the water column, whereas the lowest values (0 to 17.6 mmol O_2 m^{-3} d^{-1}) were observed between 10 and 20 m depth (Figure 8c to 8j). CR rates did not show a definite vertical pattern, registering highest (23.3 to 76.3 mmol O_2 m^{-3} d^{-1}) and lowest (0 to 12.3 mmol O_2 m^{-3} d^{-1}) values throughout the water column (0–20 m) (Figure 8c–j).

Throughout the study period in different fjords, integrated GPP and CR rates (down to 20 m) ranged from 0.1–2.6 g C m^{-2} d^{-1} and from 0.8–6.6 g C m^{-2} d^{-1}, respectively, (Figure 9, Table 2). Neither rate showed significant differences (p >0.05) between spring-summer 2020–2021 (Figure 9a) and summer of 2022 (Figure 9b). Although there were no significant differences (p >0.05) between GPP values recorded from different fjords in both study periods (Figure 9a–b), Comau Fjord showed the lowest rates of GPP (0.1 to 0.6 g C m^{-2} d^{-1}) whereas Puyuhuapi and Reloncaví fjords showed the highest values (1.9 to 2.6 g C m^{-2} d^{-1}). In the case of CR, the highest rates were recorded in Puyuhuapi Fjord (2.2 to 6.6 g C m^{-2} d^{-1}) and the lowest in Comau Fjord (0.8 to 0.9 g C m^{-2} d^{-1}) (Figure 9a, 9b). The phytoplankton composition in the study area showed a similar pattern to the GPP values, highlighting

maximum abundances on the surface and minimal abundances at a depth of 20 m (data not shown). In addition, Comau Fjord showed the lowest abundances (66 × 10^3 cell L^{-1}) whereas Reloncaví Fjord showed the highest concentrations of phytoplankton (1,227 × 10^3 cell L^{-1}).

Estimated rates of BSP ranged between 0.05 and 0.6 g C m^{-2} d^{-1} within the study area and were positively and significantly correlated with GPP values (Figure 9, Table 2). The percentage of GPP utilized by bacteria ranged from 3% to 56%, except in Comau Fjord, where a higher utilization percentage (151%) was recorded, suggesting that more organic carbon is consumed than is produced locally.

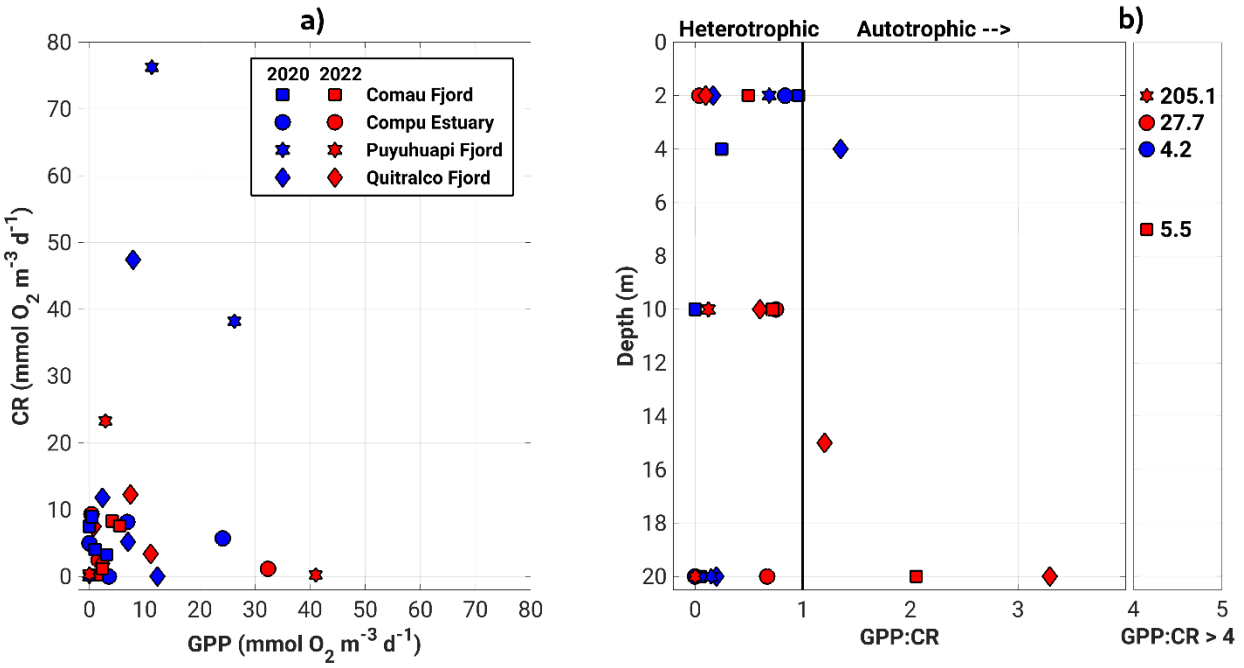

Figure 8. (a) Relationship and (b) vertical patterns of all datasets from the GPP and CR. (c−j) represents the vertical distribution of GPP and CR obtained during experiments of primary production on (c−f) spring-summer of 2020−2021, and (g−j) summer of 2022. GPP: Gross primary production, and CR: community respiration.

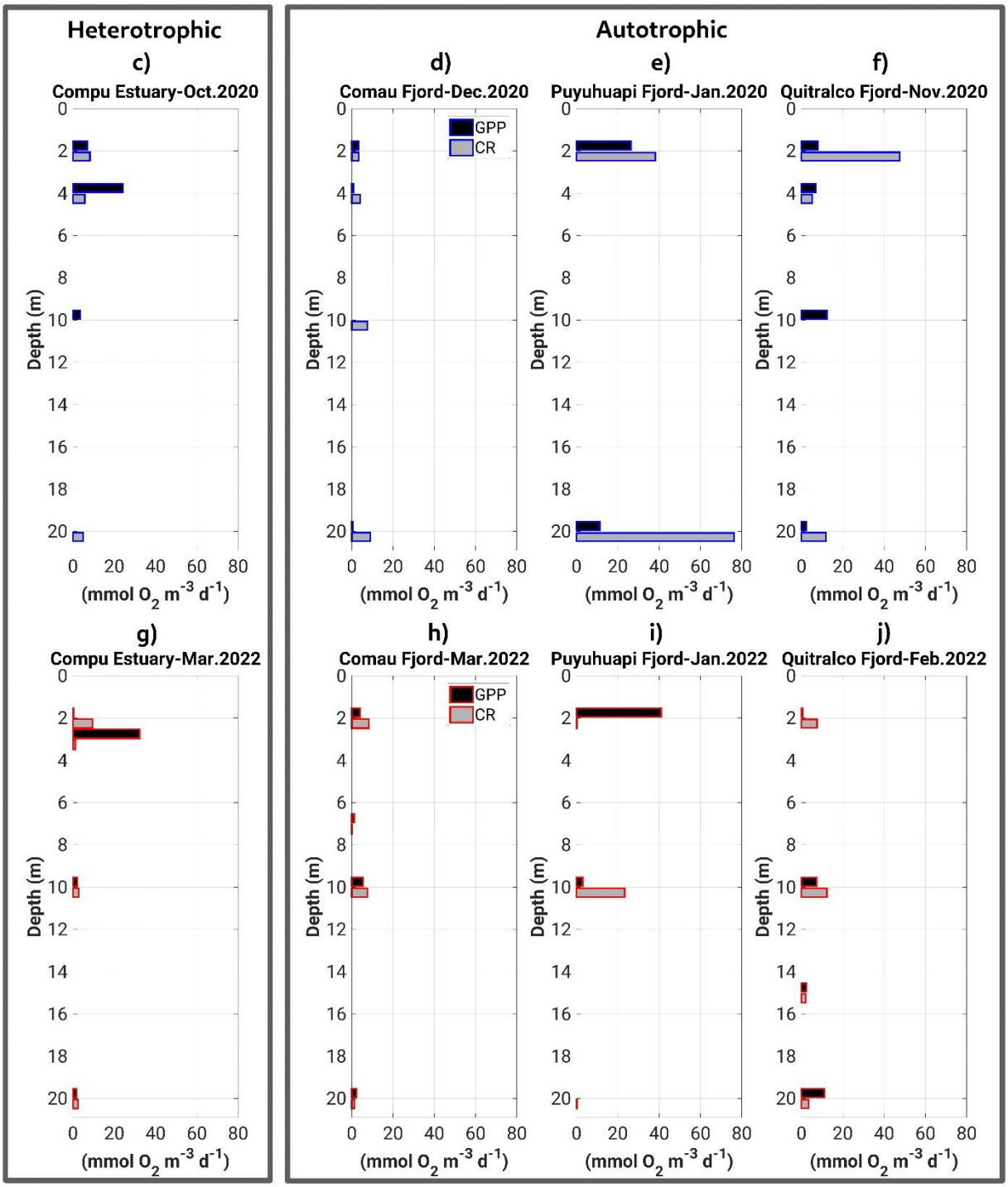

480 Figure 8. Continued.

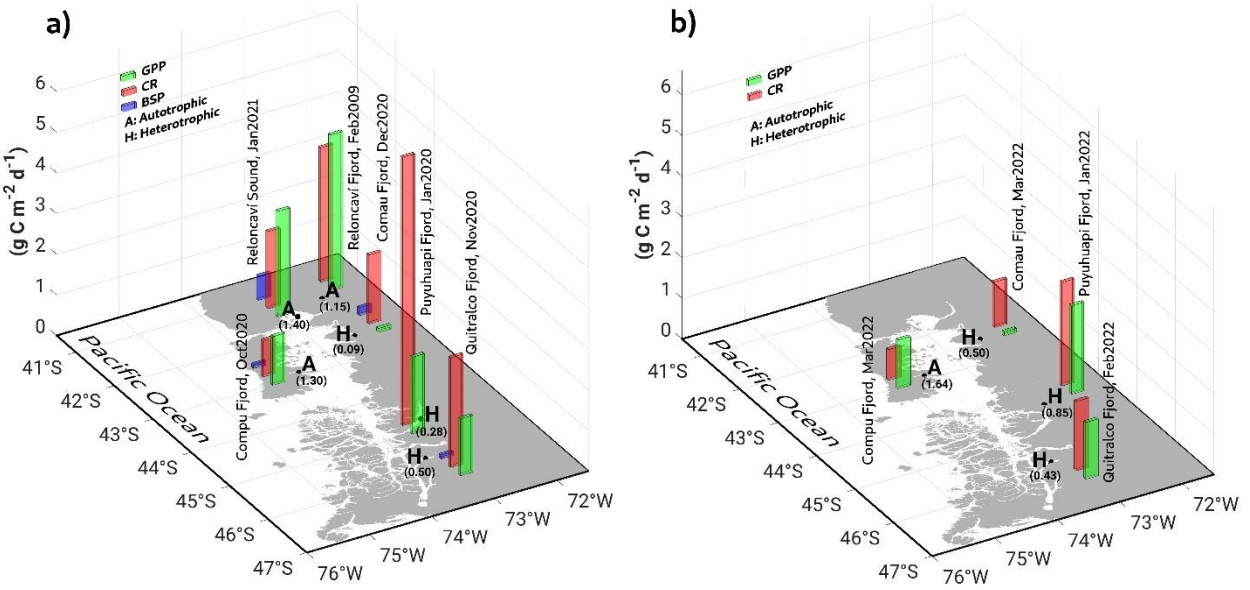

Figure 9. *In-situ* measurements of primary production during (a) spring-summer of 2020−2021, and (b) summer of 2022, covering some fjords in the northern Patagonian fjord system. GPP: Gross primary production, CR: Community respiration, BSP: Bacterial secondary production. Results shown from Reloncaví Fjord in (a) were extracted from Montero et al. (2011).

3.4. Satellite image of organic matter supply to fjords

Satellite images show that freshwater inputs into the sea were accompanied by large amounts of suspended particles (Figure 10), possibly acting as a source of allochthonous organic matter, favoring the heterotrophic metabolism reported in the previous section. On May 9, 2017, a large amount of suspended matter flowed into the Reloncaví Sound from its fjord, mainly dominated by three rivers: Petrohue, Cochamo, and Puelo (Figure 10b). In the southeast part of the Reloncaví Sound, the observed high concentration of suspended particles was accompanied by the presence of a diatom bloom (evidenced by greenish waters at the true color images in the southeast part of the Reloncaví Sound), mainly formed by *Skeletonema costatum*, which attained concentrations of more than 5 million cells L^{-1} within the fjord (Figure S8). This bloom affected both the eastern part of the Reloncaví Sound and the Reloncaví Fjord. The amount of suspended matter visible in the Sentinel-2 images was generally homogeneously high along the fjords e.g., on June 9, 2022, in the Quitralco Fjord (Figure 10c), and May 9, 2017, in Reloncaví, (Figure 10b). However, heterogeneous distribution can also be found (e.g. on April 6 2018 on Comau Fjord, Figure 10d), suggesting the influence of suspended particles within the fjord, suggesting the influence of the currents in the distribution of waters rich in sediment. On this date, waters flowing from the river Blanco in the northern part of the fjord's mouth were whitish. Water flowing into this fjord from the south, principally from the Lloncochaígua and Vodudahue rivers, has a more brownish color.

At the Quitralco Fjord (Figure 10c), SSPM from Rio de los Huemules (at 73.30° E 45.54° S, the brown riverbed is clearly visible in the natural color insert) appeared to propagate within the fjord, affecting the water clarity along the

entire fjord. Inspection on other dates (not shown) revealed high variability in the direction of the river outflow, sometimes entering the fjord (and staying there for extended periods), and sometimes being directed towards the south. Finally, the Puyuhuapi Fjord also registered a high signal from SSPM due to river discharge; for example, the Vestiquero River was located at the fjord head (Figure 10e). Other rivers, such as the Cisnes, Marta, and Uspallante, could also influence the supply of allochthonous organic matter to the Puyuhuapi Fjord, contributing to a decrease in DO and hypoxia. However, the cloud cover does not allow for better satellite images.

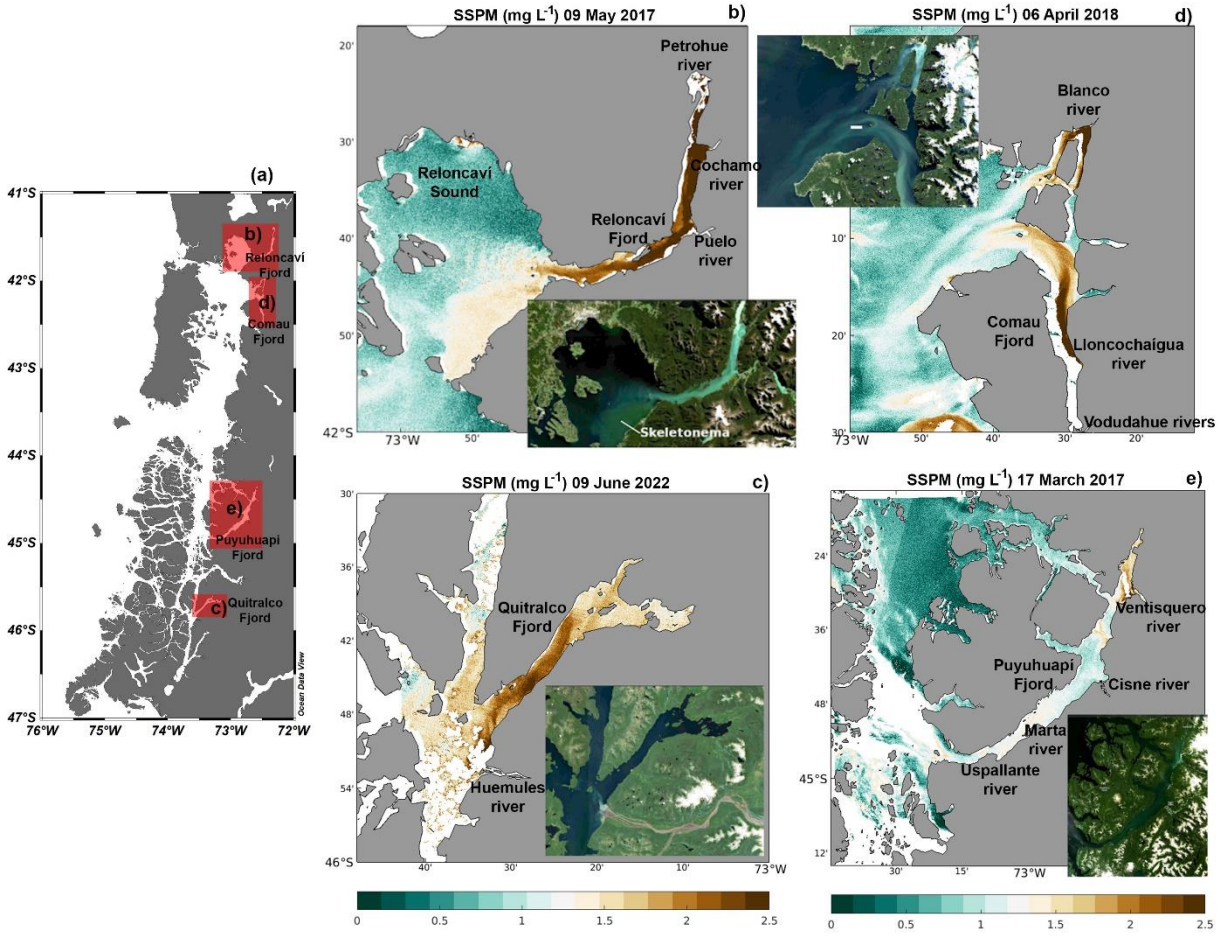

Figure 10. (a) Map showing the study sites. Satellite suspended particulate matter as measured by Sentinel 2 on (b) Reloncaví Sound, (c) Quitralco Fjord, (d) Comau Fjord, and (e) Puyuhuapi Fjord.

3.5. Biogeochemical variables

We observed different signals of SPM (Figure 11b) along a latitudinal transect conducted from north to south in the northern Patagonian fjords (Figure 11a). Specifically, significant increases in SPM were registered in Cupquelán Fjord (~ 7 mg L^{-1}) and at the surface layer of the mouths of Comau Fjord (~ 6 mg L^{-1}). Furthermore, smaller areas with values of SPM> 3 mg L^{-1} were found at the subsurface layer of the Quitralco and Aysén fjords. In

the northern region, within the Chiloé Inner Sea and the subsurface layer of the Comau and Reloncaví fjords, SPM values were minimal.

The percentage of allochthonous organic carbon (%POC_{allo}) exhibited an irregular distribution in the southern area, with surface minimums under 30% at the mouths of the Quitralco, Aysén, and Puyuhuapi fjords (Figure 11c). In the northern area, the Comau Fjord and Reloncaví Sound presented low %POC_{allo} values. Along the water column, %POC_{allo} appeared to increase with depth, reaching values of approximately 70%, except in the Inner Sea of Chiloé, where it was under 50%. The C:N ratio exhibited a discernible reduction with increasing depth along the water column in the broader study area, encompassing the Chiloé Inner Sea region and extending to the Reloncaví Fjord. Although a similar C:N ratio trend was observed in both Chiloé and Reloncaví, the predominant feature is not a uniform 'depth-dependent decrease' but rather an overall modest vertical gradient, ranging from 6–9. Furthermore, despite their comparable low C:N ratios, Chiloé and Reloncaví have differing CDOM concentrations, isotopic compositions, and POC allocations. Specifically, the Chiloé Inner Sea and Reloncaví Fjord exhibit analogous patterns of minimum C:N ratios (6-9). In addition, the subsurface regions of the Puyuhuapi and Aysén fjords register absolute maximum values (C:N>14), as depicted in Figure 11d.

The isotopic signal of the carbon ($\delta^{13}C$) increased in the same sites where %POC_{allo} decreased, with values ranging from –25‰ to –15‰ (Figure 11e). At the subsurface layer, the $\delta^{13}C$ signal became lighter than that in the surface. An exception was observed in the Chiloé Inner Sea and the transition zone between the Aysén Fjord and San Rafael Lagoon, where the C:N ratio coincidentally decreased. In the region extending from the southern Chiloé Inner Sea to Aysén Fjord, elevated levels of the isotopic signal of nitrogen ($\delta^{15}N$) enrichment were observed, primarily at the surface and subsurface levels (Figure 11f). Notably, there was a significant increase in nitrogen values, with some exceeding 9%; particularly, in the Chiloé Inner Sea, the enrichment extended to depths of 150-200 m.

The first CDOM observations in the Patagonian fjords denoted high concentrations throughout the water columns in the north area, spanning from the Chiloé Inner Sea to the Reloncaví system (Figure 11g). Conversely, in the southern area, CDOM concentrations declined, with minimum values as low as 20 μg L^{-1} of specific UV absorbance between the Jacaf Channel and San Rafael Lagoon, but the absolute minimum was registered in the Comau Fjord. Despite this overall decrease, localized increases in CDOM concentrations were identified in certain fjords, such as Aysén, Quitralco, and the San Rafael Lagoon. These subsurface concentration spikes highlight the spatial variability of CDOM distribution within the fjord system. Moreover, these findings provide valuable insights into the spatial distribution patterns of CDOM in the Patagonian fjords, indicating higher concentrations in the northern region and a decline towards the southern end of the study area. The localized increases in CDOM concentrations in specific fjords suggest the influence of local processes or inputs contributing to the observed spatial heterogeneity.

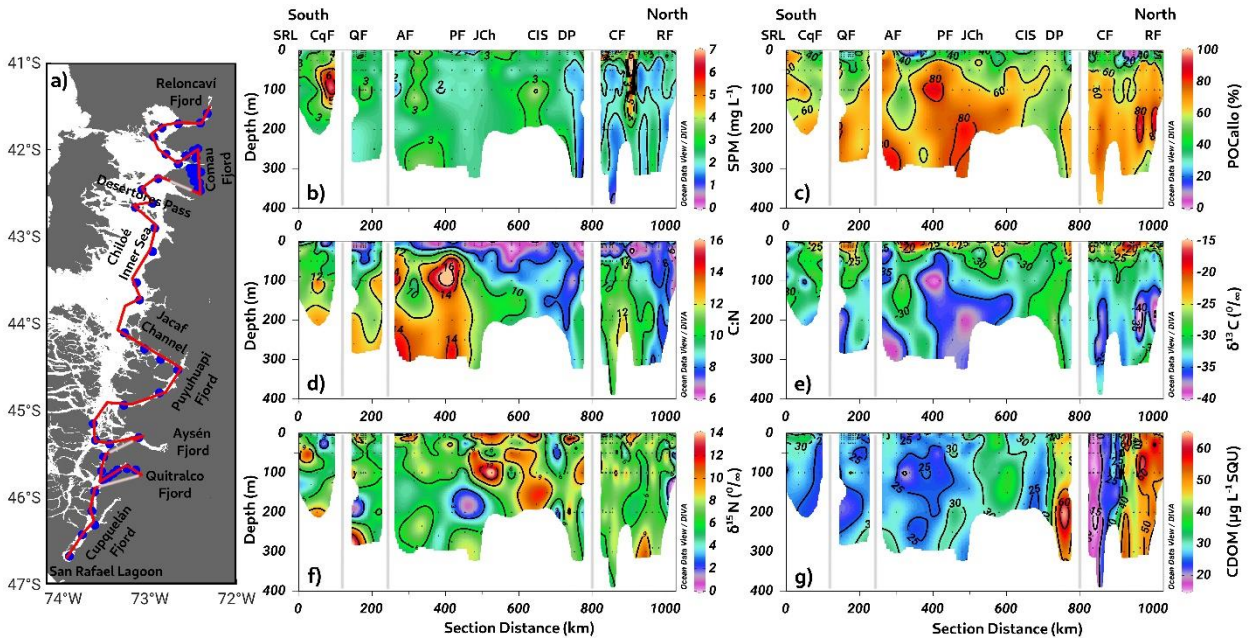

Figure 11. (a) Study area showing transects used to study biogeochemistry in November 2020 during Expeditions PN-I IFOP.. (b) Suspended particular material (SPM), (c) allochthonous carbon percentage (POC_{allo}), (d) Carbon and nitrogen ratio (C:N), Isotopic signal of (e) $\delta^{13}C$ and (f) $\delta^{15}N$, and (g) Chromophoric Dissolved Organic Matter (CDOM).

3.6. Circulation regime from ADCP measurements

The low-frequency deep circulation (> 40 m depth) in the mooring of the Corcovado Gulf showed a marked east–west direction in the along-channel current amplitude (Figure 12b). The Corcovado currents were dominated by an eastward flow with a maximum intensity of approximately 30 cm s^{-1} (Figure 12a-b), whereas at the mouth of the Puyuhuapi Fjord (Figure 12c-d), the maximum current was approximately 10 cm s^{-1}.

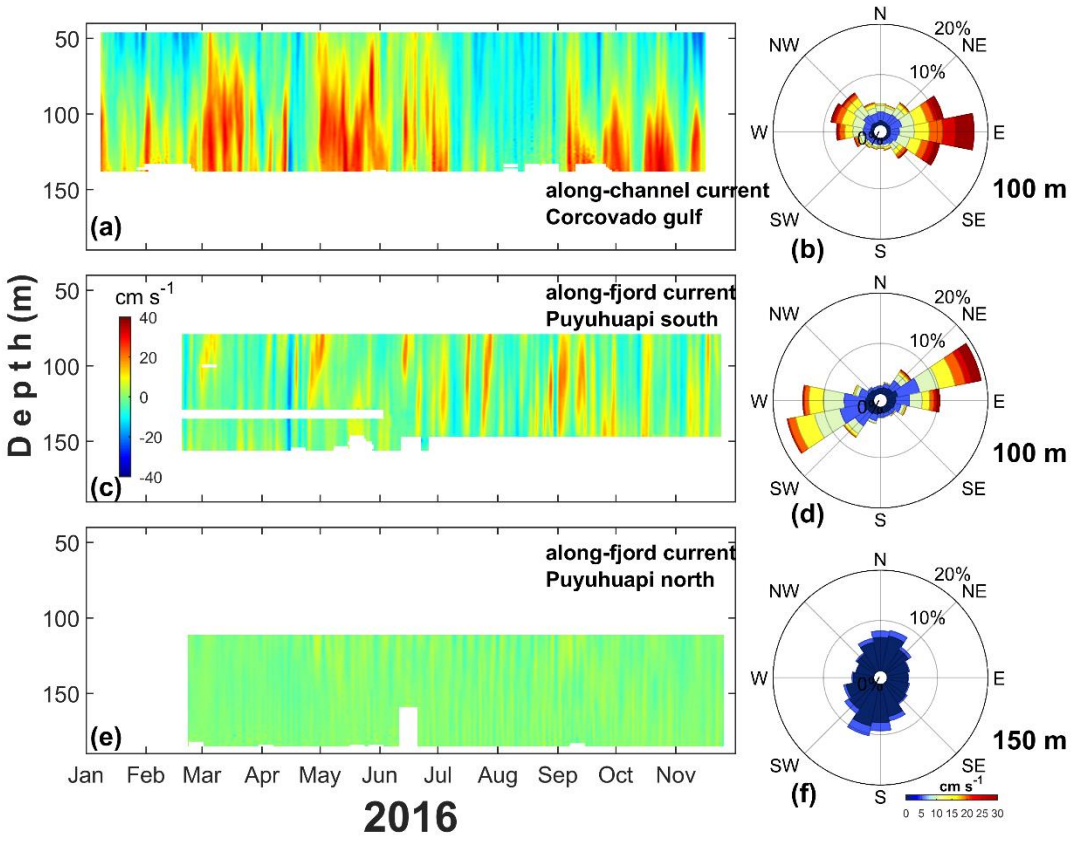

Figure 12. Subtidal deep circulation regimen obtained with ADCP performed in the (a) Corcovado Gulf and in (c, e) southern-northern zone of the Puyuhuapi Fjord from January to November 2016. (b, d, and f) Marine current rose obtained at 100 m (Corcovado Gulf), 100 m (Puyuhuapi south), and 150 m (Puyuhuapi north) depths. Location of moorings shown in Figure 1. In (a and c) the red-blue color represents the eastward-westward currents, and in (e) red-blue color represents northward-southward currents.

The Corcovado currents showed a marked pattern in the 40–70 m layer, which was dominated by westward currents, and short-duration events of approximately 20 cm s^{-1} were observed throughout the entire time series. This intense westward flow seems to be associated with the austral spring-summer seasons (January–March and November–December 2016); however, a weak (~5 cm s^{-1}) and longer (July–October 2016) westward flow was observed during the austral winter-autumn period. In the layer between 70 and 130 m, eastward (and intense) currents dominated, and there were periods of one to two months with eastward flow during March–April, May–July, and September–December 2016 with currents > 20 cm s^{-1}. The layer between 100 and 130 m showed maximum currents of approximately 40 cm s^{-1} at the end of October 2016 (Figure 12a).

Puyuhuapi Fjord currents were obtained at the southern mouth (South Puyuhuapi, Figure 12c-d) and middle fjord (North Puyuhuapi, Figure 12e-f. At the mouth of the fjord, low-frequency currents showed short pulses that covered most of the 70–160 m layer; typically, those pulses were eastward without an evident seasonal pattern. A unique low-frequency westward event was observed in mid-April 2016, which was also present in the Corcovado

Gulf. In general, the currents in southern Puyuhuapi were weak (< 10 cm s^{-1}); however, during September and October 2016, eastward events of 20 cm s^{-1} were observed. In northern Puyuhuapi, most currents were weak (< 10 cm s^{-1}) without a temporally or spatially evident pattern, and the flow tended to be northward and intensified between May and September 2016.

3.7 Circulation regimen oceanographic model

Deep subtidal currents (average of 50–300 m) over the three years of simulation, have a relatively large spatial variation (Figure 13a–b). The model could correlate the most energetic zones in the outer channels with those of lower energy inside the fjords. In general, the exchanges between the fjords and ocean registered high average velocities, that is, the Guafo mouth, Moraleda Channel, Corcovado Gulf, and Desertores Pass, with net current velocities ranging from 10 to 20 cm s^{-1}. In contrast, in the fjords, the average velocity of the deep flow was less than 5 cm s^{-1}. The predominant flow was generally towards the interior of the fjords (Figure 13–b).

The flushing/residence time calculated for each fjord showed that the sector towards the head of Puyuhuapi Fjord registered the longest retention time (>200 days). In comparison, the shortest times were found in the Reloncaví Sound−Fjord (60−90 days), except for the Reloncaví Fjord head, which reached values close to 100 days (Figures 13c and 13d). Comau Fjord showed relatively high values, which increased from mouth to head. In the central part of Comau Fjord, the residence time ranged from 90 to 120 days, whereas at the fjord head, it ranged from 150 to 190 days. Meanwhile, the Aysén Fjord showed residence time values lower than 120 days, which were higher towards the fjord head, whereas the Quitralco Fjord had residence times of 150 days at the fjord head and 100 days at its central part. Finally, the Cupquelán Fjord exhibited greater homogeneity throughout the fjord, with relatively high values ranging from 120 to 150 days. The areas of longer residence time coincided with the region of LDOW and hypoxia (Figures 13e–f).

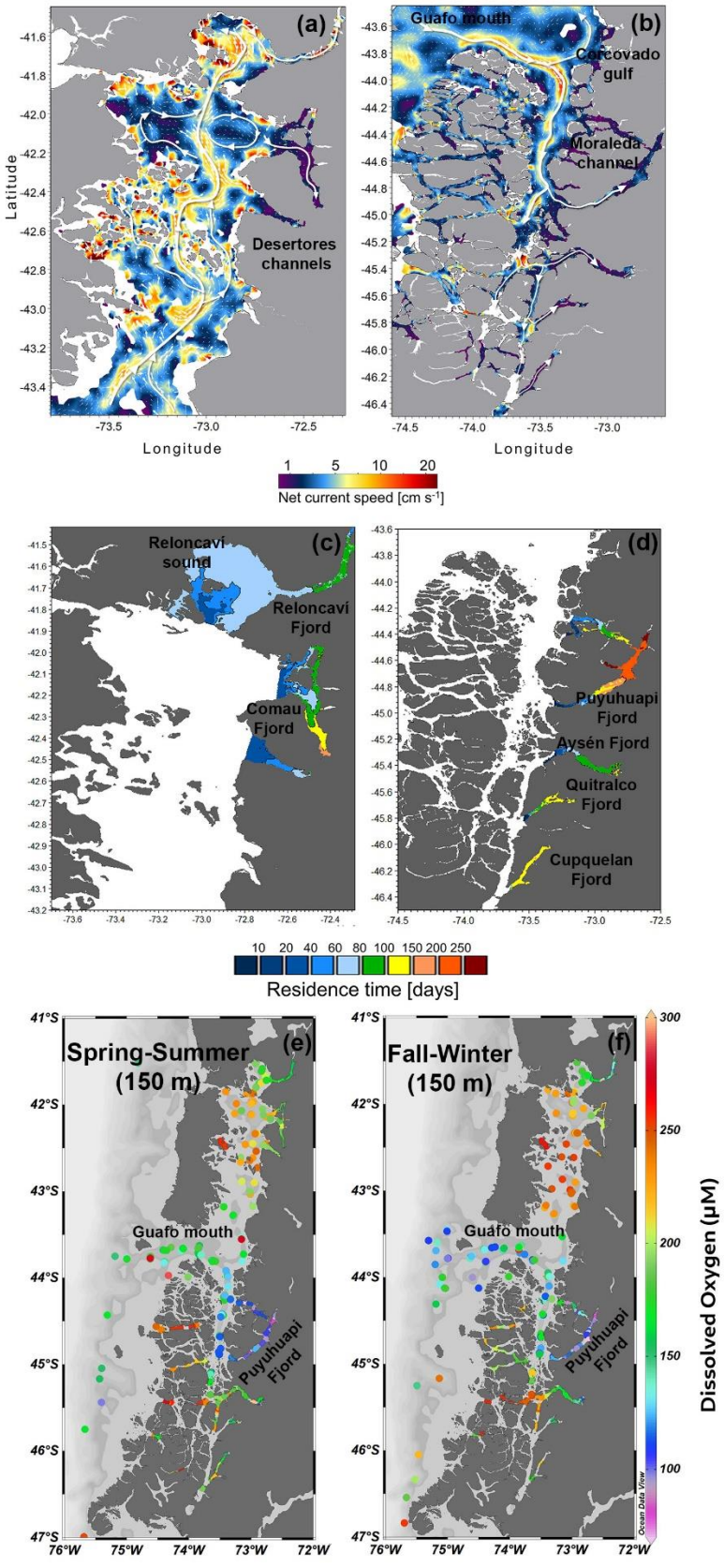
(a)
(b)
Guafo mouth
Corcovado gulf
Moraleda channel
Desertores channels
Latitude
Longitude
Longitude
1 5 10 20
Net current speed [cm s-1]
(c)
(d)
Reloncaví sound
Reloncaví Fjord
Comau Fjord
Puyuhuapi Fjord
Aysén Fjord
Quitralco Fjord
Cupquelan Fjord
10 20 40 60 80 100 150 200 250
Residence time [days]
Spring-Summer (150 m)
(e)
Fall-Winter (150 m)
(f)
Guafo mouth
Puyuhuapi Fjord
Dissolved Oxygen (µM)
Ocean Data View

Figure 13. (a, b) Map showing the deep currents regime in the northern Patagonian fjords. The deep current was defined as subtidal currents calculated as the average of currents from 50−300 m depth. (c, d) The residence time was calculated for each northern Patagonian fjord. (a-d) Data were obtained from the hydrodynamic model MIKE 3 FM developed by IFOP. (e, f) Horizontal distribution of dissolved oxygen at a level of 150 m during spring-summer and fall-winter. Data and bathymetry are plotted in color dots and gray.

4. Discussion

Oceanographic research in the Patagonian fjords started in 1995 with the CIMAR-fjords project, supported by the Chilean Navy. As an oceanographic sampling strategy, Patagonia was divided into three zones, e.g., northern (41°–47° S), central (47°–53° S), and southern (53°–55.8° S) Patagonia, and the frequency of the cruises were primarily seasonal (Sievers, 2008). Moreover, other oceanographic cruises, such as the Hudson expedition in 1970, occurred in this zone (Table 1). The data collected through the CIMAR projects allowed us to understand the main physical (water mass quantification) and chemical (e.g., dissolved oxygen and inorganic nutrients) processes impacting this fjord system, such as the hypoxic conditions due to the influence of the ESSW (Sievers, 2008; Sievers and Silva, 2008; Silva, 2008; Silva and Vargas, 2014; Schneider et al., 2014; Pérez-Santos et a., 2014). Furthermore, some studies about biological processes that include the consumption of DO, such as respiration and the remineralization of organic matter, have also contributed to understanding the processes that favor hypoxia and DO depletion (Montero et al., 2011; 2017; Iriarte et al., 2018). Additionally, the development of hydrodynamic models helped to determine the areas where the water age was significantly high, for example, the Puyuhuapi Fjord (Pinilla et al., 2020), and where stronger mixing and stratification occurred (Ruiz et al., 2021). Our study scrutinized the natural processes contributing to the presence of water under hypoxic conditions and LDOW in the northern Patagonian fjords, as discussed in the next section.

4.1 Water masses properties and biogeochemical processes in northern Patagonian Fjords

Recent and historical hydrographic data collected from the Patagonian fjords, especially in the northern area, confirmed the presence of analogous water masses detected previously by the Hudson oceanographic cruise in 1970. EW, MSAAW, SAAW, and ESSW were recorded from the surface layer to the bottom (to a depth of approximately 500 m) (Figure 2 and Figure 3). Similar patterns were recognized in terms of the vertical-horizontal distributions, highlighting the location of the salty-hypoxic/LDOW and nutrient-rich waters associated with the ESSW in the Jacaf Channel and Puyuhuapi Fjord (Figures 2 and 4). This water mass enters Patagonia within the subsurface layers via the Guafo Mouth and moves south throughout the Moraleda Channel to end at the Puyuhuapi Fjord and Jacaf Channel (Linford et al., 2023). In contrast, the EW dominated in the southern area due to freshwater input from the San Rafael Lagoon and river discharge, which is characterized by oxygenated waters due to its high solubility and recent contact with the atmosphere. Finally, SAAW and MSAAW covered the entire study area (Figure 2), as reported by Siever and Silva (2008), Schneider et al., (2014), Pérez-Santos et al., (2014), and Pinilla et al., (2020).

The absence of stratification was observed throughout the year in the Chiloé Inner Sea (Figure 5). In this area, both physical and biogeochemical variables showed homogeneous values from the surface layer to the bottom (Figures 2 and 4), indicating the presence of MSAAW (originating from mixing the SAAW with the EW). Furthermore, the calculation of the buoyancy frequency and potential energy anomalies using the output from the oceanographic model demonstrated that more robust mixing occurred in the Chiloé Inner Sea (Ruiz et al., 2021). This explains the importance of this area for DO ventilation and redistribution in the northern Patagonian fjords.

Water masses in northern Patagonia have unique physicochemical properties (Sievers and Silva, 2008; Silva, 2008; Silva and Vargas, 2014; Schneider et al., 2014; Pérez-Santos et al., 2014). In the case of northern Patagonian fjords, EW is rich in silicate (Figure 4f) because of the riverine supply (Silva and Vargas, 2014), with characteristic high spatial variability in silicate at the surface layer that changes throughout the year due to the organisms' consumption (Montero et al., 2011), as observed in northern Patagonia, including the Chiloé Inner Sea (Figure 4). Organic matter degradation processes occurred inside the fjords, mainly in terms of nitrogenous compounds being remineralized. These processes increase the nutrient pool that is originally transported by oceanic water and are responsible for the high accumulation of nitrate and phosphate registered in the subsurface layer of the Puyuhuapi Fjord and Jacaf Channel (Figure 4).

Inside the fjords, where low salinity from high river discharge dominated, a persistent halocline/pycnocline/stratified water column developed; therefore, deep-water ventilation by vertical mixing and diffusion with the oxic surface layer was limited (Figures 2–5). These conditions favored the occurrence of LDOW zones in the fjords, where stratification and particulate organic matter input were higher than at the mouths (Figure 10). Thus, DO consumption was favored owing to organic matter degradation in the Reloncaví, Comau, Puyuhuapi, Aysén, and Quitralco fjords (Figure 2), as was reported for the Milford Sound in New Zealand (Stanton, 1984), Framvaren Fjord in Norway (Yao and Millero, 1995), Lower St. Lawrence Estuary in Canada (Lefort, 2012), and Rivers Inlet in British Columbia (Jackson et al., 2022).

A latitudinal transect from north to south in the study area revealed distinct signals of SPM within the fjords. A noteworthy pattern of increased SPM levels below the surface was observed at the fjord mouths, particularly in the southern part of the study area (Figure 11b). This finding suggests that the fjord mouth plays a crucial role in particulate organic matter accumulation, potentially originating from terrestrial sources. Furthermore, the high SPM values observed in the southern region indicate substantial contributions of allochthonous material, which may be influenced by factors such as river discharge, sediment resuspension, and glacial activity (Gonzalez et al., 2010). A more detailed analysis of SPM distribution revealed irregular patterns in the percentage of allochthonous organic matter ($\%POC_{allo}$). At the mouths of the Quitralco, Aysén, and Puyuhuapi fjords, a surface minimum indicated relatively low terrestrial organic matter inputs as was reported by Gonzalez et al., (2010). The low-level input of organic matter could be attributed to limited river contributions or the autochthonous organic material production rate coinciding with nutrient depletion and increased DO (Holding et al., 2017).

In contrast, areas such as the Jacaf Channel and the Chiloé Inner Sea exhibited higher contributions of $\%POC_{allo}$, indicating a more significant influence of allochthonous sources. Further, the increase in $\%POC_{allo}$ with depth highlights the importance of vertical transport and sedimentation processes in determining the distribution of

organic matter throughout the water column (Figure 11c). Given the notable seasonality in carbon fluxes and fjord system dynamics, as highlighted by Gonzalez et al. (2010), the potential implications extend to the variability of trophic webs and carbon export. Recognizing that these effects are more autonomous from local primary production than open ocean water systems is crucial. The seasonally driven variations in carbon fluxes can significantly influence the intricate interactions within trophic webs and contribute to fluctuations in carbon export processes within the fjord system. The C:N ratio exhibited spatial variability, with more homogeneous values in surface layers shallower than 50 m (Figure 11d).

On average, the bulk particulate organic carbon and nitrogen concentrations maintained a C:N ratio of 8.5:1, exceeding the Redfield ratio of 6.6:1 typically observed in phytoplankton biomass within the marine realm (Redfield, 1958). Notably, the southern region exhibited higher C:N ratios, coinciding with areas with elevated SPM levels and increased $\%POC_{allo}$. While the intuitively higher C:N ratio could be attributed to terrestrial sources with a higher carbon-to-nitrogen content, a more plausible explanation could be the increasing trend of the C:N ratio with depth and elevated particulate organic carbon (POC_{allo}), or a combination of both. The observed C:N ratios suggest the influence of microbial remineralization processes and the preferential removal of nitrogen-rich organic matter (Taucher et al., 2020), potentially result in a lower POC_{allo} signal. The increase of the C:N ratio with depth likely reflects the consumption and degradation of sinking particles by zooplankton and heterotrophic bacteria, resulting in the preferential remineralization of nitrogen (Figure 3) over carbon and the subsequent elevation of the C:N ratio in sinking particles (Tomas et al., 1999; Schneider et al., 2003).

The spatial gradients of $\delta^{13}C$ have been previously documented in estuarine and continental shelf waters in Patagonian fjords (Silva and Vargas, 2014 Gonzalez et al., 2010; Iriarte et al., 2018). The horizontal–vertical distribution of the isotopic signal of $\delta^{13}C$ and $\delta^{15}N$ showed substantial variability in the northern Patagonian fjords and, for the first time, is before reported for the $\delta^{15}N$. The pronounced phytoplankton bloom (Figure 7b) resulted in an enrichment of $\delta\ ^{13}C$ in the upper 50 m of SPM (Figure 11e), similar to observations made in other fjords around the world (Remeikaite-Nikiene et al., 2017). The isotopic carbon signals revealed an increase in $\delta^{13}C$ values where $\%POC_{allo}$ decreased, indicating a shift towards a more depleted isotopic signature. This suggests the predominance of marine-derived organic carbon in areas with lower inputs of allochthonous material (Kumar et al., 2016). Moreover, the lighter carbon isotopic signals observed with depth suggest isotopic fractionation processes associated with remineralization and the preferential utilization of more labile organic carbon by heterotrophic bacteria (Muñoz et al., 2014; Kuliński et al., 2014).

The seasonal distribution of Chl-a evidenced the phytoplankton activity along the northern Patagonian fjords, especially during spring, 2020 (Figure 7). However, in the winter of 2021, a phytoplankton bloom was registered in the Reloncaví Fjord and Ancud Gulf. Pérez-Santos et al., (2021) reported the occurrence of high Chl-a and an increase of phytoplankton in the Reloncaví Sound during middle and late winters (August and September, 2017–2020) due to changes in the water column conditions, e.g., stratification started when salinity decreased owing to the increase of river discharge mainly caused by early start of the ice melting. The stabilization of the water column is one of the main factors triggering primary production in the Patagonian fjords (Pérez-Santos et al., 2021).

Elevated levels of nitrogen enrichment were primarily observed in the surface layer of the region extending from the southern Chiloé Inner Sea to the Aysén Fjord, indicating the influence of nitrogen inputs from sources such as river discharge, atmospheric deposition, and biological activity (Velinsky and Fogel, 1999). The significant increase in nitrogen values, particularly in the Chiloé Inner Sea, suggests the presence of enhanced nitrogen cycling and retention processes within this fjord system. This increase could result from the degradation of organic nitrogen with depth, where isotopically light $\delta^{15}N$ is preferentially released from the organic matrix, leaving behind isotopically heavier residual $\delta^{15}N$ (Saino and Hattori, 1980, 1987; Altabet, 1988). Similarly, the enrichment of $\delta^{15}N$ in SPM suggests that primary production mainly originates from autochthonous sources in some regions of the fjords (Figure 11). The horizontal–vertical distribution of the isotopic signal of $\delta^{13}C$ and $\delta^{15}N$ showed substantial variability in the northern Patagonian fjords. Our results strongly suggest that this variability was driven by biological processes, as was demonstrated by Savoye et al. (2003). They found that the co-variation of $\delta^{13}C$ and $\delta^{15}N$ reflects the seasonal succession of phytoplankton species due to seasonal changes in abiotic factors, such as temperature and nutrient concentration.

The distribution of CDOM in the Patagonian fjords reveals distinctive patterns, as depicted in Figure 11. Notably, elevated CDOM concentrations were observed in the northern region, likely stemming from increased terrestrial inputs, heightened microbial activity, and prolonged CDOM residence times (Figure 13). This phenomenon aligns with observations in fjords within the northern hemisphere (Mannino et al., 2008). Conversely, the southern region displays lower CDOM concentrations, indicative of diminished dissolved terrestrial inputs and potentially more efficient removal processes. The proposal that localized CDOM concentration peaks within specific fjords signify the influence of local processes, including freshwater inputs, glacier melting, or biological production (Mannino et al., 2008), contributing significantly to the spatial heterogeneity of CDOM distribution in Patagonian fjords.

4.2. Mechanisms driving hypoxia and LDOW in northern Patagonian fjords

As discussed in the previous section, one of the principal mechanisms involved in the origin of hypoxic conditions in some areas of the northern Patagonian fjords was attributed to the advection of the ESSW from the Pacific Ocean to Patagonia. Recently, Linford et al. (2023) demonstrated the poleward advection of water with lower DO values by the ESSW that was transported by the Perú Chile Undercurrent (PCUC). The passage of this water mass into the northern Patagonian fjord system was detected in a DO time series from a mooring system installed at the Guafo mouth. Moreover, as shown in Figure 2, extreme hypoxic conditions were registered in the Quitralco Fjord, where ESSW was absent (Figure 6d-f).

In the Quitralco Fjord, the DO concentration was mainly governed by the biological processes of oxygen production and consumption during photosynthesis and respiration, respectively. The primary production experiments conducted in this fjord (Figures 8 and 9) showed higher values of community respiration than the primary production of DO (Table 2). In addition, the oceanographic model showed a less intense deep net current, allowing a residence time of water between 100−150 days (Figure 13). Furthermore, satellite images provide evidence of a high concentration of suspended sediments along the Quitralco Fjord due to river discharge (Figure

10). Regarding Magdalena Sound, the shallower hypoxia observed there (70 m depth) could be explained by the occurrence of the local upwelling produced when westerly winds blow across the mountains, as reported for the Comau Fjord by Crosswell et al. (2022) and Díaz et al. (2023), and to a temperate Canadian Fjord (Jackson et al., 2023). A shallower hypoxia (10−20 m) was also registered in Clayoquot Sound, British Columbia, mainly attributed to local processes, such as, DO consumption during the organic matter degradation, enhanced by upwelling conditions (Rosen et al., 2022).

DO concentrations in the water column are modulated by biological processes via photosynthesis (i.e. through oxygen production) and respiration/remineralization (e.g. oxygen consumption), as well as by the physiochemical properties of water (Zhang et al., 2010). In general, the production of oxygen occurs through photosynthesis in the surface waters (euphotic zone) and oxygen consumption occurs through respiration and remineralization in the entire water column. Consequently, surface waters usually contain high concentrations of oxygen as a result of photosynthesis and atmospheric exchange, whereas concentration decreases in deeper waters (Pitcher et al. 2021). In coastal waters or fjord ecosystems, owing to the high amount of organic matter (autochthonous and allochthonous) available in the water column, a greater amount of oxygen is consumed (Jackson et al., 2022) during microbial respiration (Robinson, 2019), thus dominating heterotrophic processes over autotrophic processes. Nevertheless, seasonal and spatial differences can also be observed in the dominance of these processes. This study recorded high CR rates (greater than GPP), indicating heterotrophic metabolism, where more oxygen was consumed than produced (Figure 8). Nevertheless, Puyuhuapi Fjord, and Compu estuary showed high oxygen production values (GPP >20 mmol O_2 m^{-3} d^{-1}) within the 2-m to 4-m layer at least in one of the two sampling periods (Figure 8), suggesting a greater uptake than release of CO_2 due to the high surface primary production rates during the spring-summer period at surface waters of some Patagonian fjords (Torres et al., 2011). A recent global assessment of CO_2 uptake from estuaries, including tidal systems and deltas, lagoons, and fjords reported that fjord ecosystems can reduce 37% of CO_2 anthropogenic emissions (Rosentreter et al., 2023). DO and organic matter are produced only in the well-lit upper ocean but can be consumed throughout the water column. Therefore, in areas of high surface production and slow resupply of oxygen at depth (compared to the rate at which oxygen is respired), DO concentrations may be reduced to hypoxic levels at depth. Nevertheless, sporadic deepwater renewal was observed close to the bottom (160−180 meters) in Puyuhuapi Fjord owing to the inflow of dense water above the sill favoring the ventilation and inhibiting the occurrence of deep anoxia conditions (Pinilla et al., 2020), as also reported by Jackson et al., (2022) in Rivers Inlet, British Columbia, and on the west coast of the Vancouver Island (Thomson et al., 2017). The first map of residence time in the northern Patagonian fjord showed a coincidence of the area where a high residence time was reported (100−250 days) with the depleted oxygen region, for example, hypoxic and LDOW areas (Figure 13). The hydrodynamic model and derived calculations are helpful tools for explaining the oxygen distribution and patterns in the northern Patagonian fjord system.

5. Conclusions

Since the beginning of oceanographic research in the Patagonian fjords (1970), hypoxia and LDOW have been reported along the water column. A dataset of hydrographic-biogeochemical parameters, *in-situ* experiments of primary production/community respiration, satellite-suspended particulate matter, and the output of a hydrodynamic

model allowed for a holistic evaluation of the oceanographic and biogeochemical processes contributing to hypoxia and LDOW in Patagonian subsurface waters. The influence of the ESSW was recognized as one of the first drivers of this phenomenon. This water mass transported poleward poorly oxygenated waters that entered the northern Patagonian fjords through the Guafo mouth and moved southward through the Moraleda and Jacaf channels and the Puyuhuapi Fjord. The distribution of the ESSW inside the northern Patagonian fjords coincides with the most extensive zone of the LDOW records. However, the hypoxic conditions registered in this zone were also attributed to the high rate of DO consumption during community respiration processes, owing to the entrance of allochthonous organic matter (natural and/or anthropogenic) to the fjords. Additionally, the results from marine currents derived from ADCP measurements and the hydrodynamic model demonstrated a weak water circulation and a long residence time leading to slow deep-water ventilation, resulting in a drop in DO level, and finally, the occurrence of hypoxic conditions. The Quitralco Fjord also reported hypoxic conditions showing the absolute minimum of DO with 9.36 μmol L^{-1} and 1.6% oxygen saturation. ESSW was not observed in this area. Therefore, the presence of hypoxic water in the deep layer of Quitralco was attributed to weak deep-water circulation and a long residence time, together with a high rate of DO consumption by community respiration and a higher supply of allochthonous organic matter due to river discharge. Similar processes favoring LDOW were registered at the Aysén, Comau, and Reloncaví fjords, but in the Reloncaví systems, marine currents and residence time were significantly higher than in other fjords. The presence of LDOW in the Reloncaví systems responded mainly to biological processes, e.g., DO consumption during community respiration by phytoplankton and remineralization by bacteria. The analyses of the processes contributing to hypoxic conditions and LDOW in the water column of northern Patagonian fjords allowed for the identification of the main causes leading to oxygen loss in each fjord investigated. The results provide the environmental information needed to contribute to the sustainable management of the northern Patagonian fjord under anthropogenic activities and climate change scenarios. In addition, it provides significant information for understanding the life cycle of marine species that inhabit Patagonian fjords. Finally, our study provides valuable insights into the relationship between hypoxia, low oxygen processes, the origin of organic carbon, isotopic signals of carbon and nitrogen, the C:N ratio, and the presence of CDOM in the Patagonian fjords. These findings highlight the complex interactions between terrestrial and marine processes and emphasize the role of fjords as potential sites for hypoxia and the accumulation of organic matter. Understanding these relationships is crucial for accurately assessing the impact of low oxygen processes and carbon cycle dynamics in fjord ecosystems and their contribution to the global carbon cycle. Further research is needed to elucidate the mechanisms driving these patterns and their implications for the functioning and resilience of fjord ecosystems against continuous environmental changes.

Data availability. All data sets used in this manuscript can be requested from the corresponding author.

Author contributions. PL: study design, data analysis, and manuscript leader. IPS: study design, collection, and analysis of physical oceanographic data, and manuscript leader. PM: study design, collection, and analysis of primary production data. PD: study design, collection, and analysis of physical-biological oceanographic data. CA: collection, and analysis of primary production data. EP: developed of oceanographic model and analysis of physical oceanographic data. FB: collection, and analysis of biogeochemical data. MC: analysis of marine current data. AA:

study design, collection, and analysis of satellite data. MA: collection and analysis of marine current data. GS: study design, collection, and analysis of physical oceanographic data. CP: edition and analysis of satellite data. CS: collection, and analysis of physical oceanographic data. SA: collection, and analysis of biogeochemical data. PN: collection, and analysis of biogeochemical data. GM: collection of physical, biological, and biogeochemical data. RA: collection of physical, biological, and biogeochemical data. JSM: processing and analysis of model data for resident time. CSR: validation hydrodynamics model. All authors contributed to the writing of the manuscript.

Competing interests. The authors declare that they have no conflict of interest.

Acknowledgments.

This research was funded by FONDECYT 1211037 and partially funded by COPAS Sur-Austral ANID AFB170006, the Office of Naval Research grant N00014-17-1-2606, COPAS COASTAL FB210021, and CIEP R20F002. Facundo Barrera was founded by FONDECYT 31308. Cécile Pujol was financially supported by the F.R.S-FNRS (Fonds de la Recherche Scientifique de Belgique, Communauté Française de Belgique) through a FRIA grant. Patricio A. Díaz was funded by Centre for Biotechnology and Bioengineering (CeBiB) (PIA project FB0001, ANID, Chile). M.I. Castillo was funded by CS2018-7929 and ATE220033. We also thank the Chonos initiative of the Instituto de Fomento Pesquero (IFOP) for facilitating the use of its computer systems to access the MIKE 3, WRF, and FLOW models and the Ministry of Economy, Development and Tourism of the Chilean Government for funding through the Undersecretary of Fisheries and Aquaculture. Elias Pinilla would like to acknowledge funding from the National Science Foundation (NSF Grant Number 2045866).

References

Aiken, C.M.: Seasonal thermal structure and exchange in Baker Channel, Chile, Dynamics of Atmospheres and Oceans, 58, 1–19, https://doi.org/10.1016/j.dynatmoce.2012.07.001, 2012.

Andrejev, O., Myrberg, K., and Lundberg, P. A.: Age and renewal time of water masses in a semi-enclosed basin—application to the Gulf of Finland, Tellus A: Dynamic Meteorology and Oceanography, 56, 5, 548-558, doi:10.3402/tellusa.v56i5.14435, 2004.

Altabet, M.A.: Variations in nitrogen isotopic composition between sinking and suspended particles: implication for nitrogen cycling and particle transformation in the open ocean. Deep-Sea Res. 35, 535–554, 1988.

Andrewartha, H. G., and Birch, L. C.: The ecological web: more on the distribution and abundance of animals, University of Chicago Press, 1986.

Barrera, F., Lara, R. Krock, J.: Factors influencing characteristics and distribution of organic particles and macromolecules in the Pacific-Atlantic connection, J. Mar. Syst., 175, 36-45, doi:10.1016/j.jmarsys.2017.07.004, 2017.

Batiuk, R. A., Breitburg, D. L., Diaz, R. J., Cronin, T. M., Secor, D. H., and Thursby, G.: Derivation of habitat-specific dissolved oxygen criteria for Chesapeake Bay and its tidal tributaries, Journal of Experimental Marine Biology and Ecology, 381, S204-S215, doi:10.1016/j.jembe.2009.07.023, 2009.

Bianchi, T. S.: Biogeochemistry of estuaries. Oxford University Press on Demand, 2007.

Bianchi, T.S., DiMarco, S.F., Cowan, J.H., Hetland, R.D., Chapman, P., Day, and Allison, J.W.: The science of hypoxia in the Northern Gulf of Mexico: A review, Science of The Total Environment, 408, 7, 1471–1484, https://doi.org/10.1016/j.scitotenv.2009.11.047, 2010.

Billi, M., Mascareño, A., Henríquez, P. A., Rodríguez, I., Padilla, F., and Ruz, G. A.: Learning from crises? The long and winding road of the salmon industry in Chiloé Island, Chile, Marine Policy, 140, 105069, doi:10.16/j.marpol.2022.105069, 2022.

Breitburg, D. L., Loher, T., Pacey, C. A., and Gerstein, A.: Varying effects of low dissolved oxygen on trophic interactions in an estuarine food web, Ecological Monographs, 67, 4, 489-507, doi:10.1890/0012-9615(1997)067[0489:VEOLDO]2.0.CO;2, 1997.

Breitburg, D., Levin, L. A., Oschlies, A., Grégoire, M., Chavez, F. P., Conley, D. J., ... and Zhang, J.: Declining oxygen in the global ocean and coastal waters, Science, 359, 6371, doi:10.1126/science.aam7240, 2018.

Castillo, M. I., Cifuentes, U., Pizarro, O., Djurfeldt, L., and Caceres, M.: Seasonal hydrography and surface outflow in a fjord with a deep sill: the Reloncaví fjord, Chile, Ocean Science, 12, 2, 533-544, doi:10.5194/os-12-533-2016, 2016.

Carrasco, C., Silva, N.: Comparación de las características oceanográficas físicas y químicas presente en la zona de Puerto Montt a la boca del Guafo entre el invierno y la primavera de 2004 y entre las primaveras de 1995 y 2004. Cienc. Tecnol. del Mar 33 (2), 17–44, 2010.

Conley, D. J., Paerl, H. W., Howarth, R. W., Boesch, D. F., Seitzinger, S. P., Havens, K. E., ... and Likens, G. E.: Controlling eutrophication: nitrogen and phosphorus, Science, 323, 5917, 1014-1015, doi:10.1126/science.1167755, 2009.

Crosswell, J.R., Bravo, F., Pérez-Santos, I., Carlin, G., Cherukuru, N., Schwarger, C., et al.: Geophysical controls on metabolic cycling in three Patagonian fjords. Prog. Oceanogr. 207, 102866, 2022.

Davis, J. C.: Minimal dissolved oxygen requirements of aquatic life with emphasis on Canadian species: a review, Journal of the Fisheries Board of Canada, 32, 12, 2295-2332, doi:10.1139/f75-268, 1975.

Diaz, R. J., and Rosenberg, R.: Marine benthic hypoxia: a review of its ecological effects and the behavioural responses of benthic macrofauna, Oceanography and marine biology, An annual review, 33, 245, 03, 1995.

Diaz, R. J.: Overview of hypoxia around the world, Journal of environmental quality, 30, 2, 275-281, doi:10.2134/jeq2001.302275x, 2001.

Díaz, P., Pérez-Santos, I., Álvarez, G., Garreaud, R., Pinilla, E., Díaz, M., Sandoval, A., Araya, M., Álvarez, F., Rengel, J., Montero, P., Pizarro, G., López, L., Iriarte, L., Igor, G., Reguera, B.: Multiscale physical background to an exceptional harmful algal bloom of Dinophysis acuta in a fjord system. Sci. Total Environ. 773, 145621 https://doi.org/10.1016/j.scitotenv.2021.145621, 2021.

Díaz, P. A., Pérez-Santos, I., Basti, L., Garreaud, R., Pinilla, E., Barrera, F., ... and Figueroa, R. I.: The impact of local and climate change drivers on the formation, dynamics, and potential recurrence of a massive fish-killing microalgal bloom in Patagonian fjord, Science of The Total Environment, 865, 161288, doi:10.16/j.scitotenv.2022.161288, 2023.

DHI: Mike 3, User Guide and Reference Manual. Danish Hydraulic Institute, Denmark, 2019.Ekau, W., Auel, H., Pörtner, H. O., and Gilbert, D.: Impacts of hypoxia on the structure and processes in pelagic communities (zooplankton, macro-invertebrates and fish), Biogeosciences, 7, 5, doi:10.5194/bg-7-1669-2010, 1669-1699, 2010.

Fuenzalida, R., Schneider, W., Garcés-Vargas, J., Bravo, L., and Lange, C. : Vertical and horizontal extension of the oxygen minimum zone in the eastern South Pacific Ocean, Deep Sea Research Part II: Topical Studies in Oceanography, 56, 16, 992-1003, doi:10.1016/j.dsr2.2008.11.001, 2009.

Fry, B., and Sherr, E. B.: δ13C measurements as indicators of carbon flow in marine and freshwater ecosystems. Ecol. Stud. 68, 196–229. doi: 10.1007/978-1-4612-3498-2_12, 1989.

Garcon V., Dewitte B., Goubanova C. and Montes I.: Land-sea-atmosphere interactions exacerbating ocean deoxygenation in Eastern Boundary Upwelling Systems (EBUS), in 'Laffoley, D. and Baxter, J.M. (eds.). Ocean deoxygenation: Everyone's problem - Causes, impacts, consequences and solutions, Gland, Switzerland: IUCN. xxii+562pp, available at: https://portals. iucn. org/library/sites/library/files/documents/03.420 DEOX. Pdf, 2019.

González, H. E., Calderón, M. J., Castro, L., Clement, A., Cuevas, L. A., Daneri, G., ... and Molinet, C.: Primary production and plankton dynamics in the Reloncaví Fjord and the Interior Sea of Chiloé, Northern Patagonia, Chile, Marine Ecology Progress Series, 402, 13-30, doi:10.3354/meps08360, 2010.

González, H. E., Nimptsch, J., Giesecke, R., and Silva, N.: Organic matter distribution, composition and its possible fate in the Chilean North-Patagonian estuarine system, Science of the Total Environment, 657, 1419-1431, doi:10.1016/j.scitotenv.2018.11.445, 2019.

Grasshoff, K., Ehrhardt, M., and Kremling, K. Methods of Seawater Analysis. (2nd edition), Verlag Chemie Weinhein, New York, USA, 1983.

Grasshoff, K., Kremling, K., and Ehrhardt, M. (Eds.).: Methods of seawater analysis, John Wiley and Sons, 2009.

Harmelin-Vivien, M., Loizeau, V., Mellon, C., Beker, B., Arlhac, D., Bodiguel, X., et al.: Comparison of C and N stable isotope ratios between surface particulate organic matter and microphytoplankton in the Gulf of lions (NW Mediterranean). Cont. Shelf Res. 28, 1911–1919. doi: 10.1016/j.csr.2008.03.002, 2008.

Herrmann, R. B.: Growth of juvenile coho salmon at various concentrations of dissolved oxygen, 1958.

Hoos, L.M.: A study of the benthos of an anoxic marine basin and factors affecting its distribution, M. Sc. Thesis, Dalhousie University, Halifax, NS. 149, 1973.

Holding, J.M., Duarte, C.M., Delgado-Huertas, A., Soetaert, K., Vonk, J.E., Agustí, S., Wassmann, P. and Middelburg, J.J.: Autochthonous and allochthonous contributions of organic carbon to microbial food webs in Svalbard fjords. Limnol. Oceanogr., 62: 1307-1323. https://doi.org/10.1002/lno.10526, 2017.

Guzmán D & Silva N.: Caracterización física y química y masas de agua en los canales australes de Chile entre boca del Guafo y estero Elefantes (crucero CIMAR 4 Fiordos). Cienc. Tecnol. Mar, 25(2): 45-76, 2002.

IOC, S.: IAPSO: The international thermodynamic equation of seawater–2010: Calculation and use of thermodynamic properties, Intergovernmental Oceanographic Commission, Manuals and Guides No. 56, UNESCO, Manuals and Guides, 56, 1-196, 2010.

Iriarte, J. L.: Natural and human influences on marine processes in Patagonian Subantarctic coastal waters, Frontiers in Marine Science, 5, 360, doi:10.3389/fmars.2018.00360, 2018.

Iriarte, J.L., Gonzalez, H.E., Liu, K.K., Rivas, C., and Valenzuela, C.P.: Spatial and temporal variability of chlorophyll and primary productivity in surface waters of southern Chile. Estuarine. Coast. Shelf Sci. 74, 471e480, https://doi.org/10.1016/j.ecss.2007.05.015, 2017.

Jackson, J. M. Johannessen S., Belluz J., Hunt B., and Hannah C.: Identification of a Seasonal Subsurface Oxygen Minimum in Rivers Inlet, British Columbia, Estuaries and Coasts, 45:754–771, https://doi.org/10.1007/s12237-021-00999-y, 2022

Jackson, J. M., Holmes, K., Klymak, J.M., Bianucci, L., Evans, W., Floyd, W.C., Hannah, C., Hare, A., and Wan, D.: Winter Arctic outflow winds cause upper ocean cooling and reoxygenation in a temperate Canadian fjord. Geophysical Research Letters, 50, e2023GL104549. https://doi.org/10.1029/2023GL104549, 2023.

Kattner, G., and Becker, H.: Nutrients and organic nitrogenous compounds in the marginal ice zone of the Fram Strait, Journal of Marine Systems, 2, 3-4, 385-394, doi:10.1016/0924-7963(91)90043-T, 1991.

Kumar, V., Tiwari, M., Nagoji, S. et al.: Evidence of Anomalously Low δ13C of Marine Organic Matter in an Arctic Fjord. Sci Rep 6, 36192, https://doi.org/10.1038/srep36192, 2016.

Kuliński, K., Kędra, M., Legeżyńska, J., Gluchowska, M., & Zaborska, A.: Particulate organic matter sinks and sources in high Arctic fjord. Journal of Marine Systems, 139, 27–37. doi:10.1016/j.jmarsys. 2014.04.018, 2014.

Kutty, M. N.: Respiratory quotients in goldfish and rainbow trout, Journal of the Fisheries Board of Canada, 25, 8, 1689-1728, doi:10.1139/f68-150, 1968.Laffoley, D., and Baxter, J. M.: Ocean deoxygenation: Everyone's problem-Causes, impacts, consequences and solutions, Gland, Switzerland: IUCN, doi:10.2305/IUCN.CH.2019.13.en, 2019.

Lefort, S.: A multidisciplinary study of hypoxia in the deep water of the Estuary and Gulf of St. Lawrence: Is this ecosystem on borrowed time?, McGill University (Canada), 2012.

Linford, P., Pérez-Santos, I., Montes, I., Dewitte, B., Buchan, S., Narváez, D., et al.: Recent deoxygenation of Patagonian fjord subsurface waters connected to the Peru–Chile undercurrent and equatorial subsurface water variability. Global Biogeochemical Cycles, 37, e2022GB007688. https://doi. org/10.1029/2022GB007688, 2023.

Mannino A., Russ M. E., Hooker S. B.: Algorithm development and validation for satellite-derived distributions of DOC and CDOM in the U.S. Middle Atlantic Bight, J. Geophys. Res., 113, C07051, doi:10.1029/2007JC004493, 2008.

Mardones, J.I., Paredes, J., Godoy, M., Suarez, R., Norambuena, L., Vargas, V., Fuenzalida, G., Pinilla, E., Artal, O., Rojas, X., Dorantes-Aranda, J.J., Lee Chang, K.J., Anderson, D.M., and Hallegraeff, G.M.: Disentangling the environmental processes responsible for the world's largest farmed fish-killing harmful algal bloom: Chile, 2016. Sci. Total Environ. 766, 144383 https://doi.org/10.1016/j, 2021.

Martínez, D., De Lázaro, O., Cortés, P., Oyarzún-Salazar, R., Paschke, K., and Vargas-Chacoff, L.: Hypoxia modulates the transcriptional immunological response in Oncorhynchus kisutch, Fish and Shellfish Immunology, 106, 1042-1051, doi:10.16/j.fsi.2020.09.025, 2020.

Meire, L. K. E. R., Soetaert, K. E. R., and Meysman, F. J. R.: Impact of global change on coastal oxygen dynamics and risk of hypoxia, Biogeosciences, 10, 4, 2633-2653, doi:10.5194/bg-10-2633-2013, 2013.

Monsen, N. E., Cloern, J. E., Lucas, L. V., and Monismith, S. G.: A comment on the use of flushing time, residence time, and age as transport time scales, Limnology and oceanography, 47, 5, 1545-1553, doi:10.4319/lo.2002.47.5.1545, 2002.

Montero, P., Daneri, G., Gonzalez, H. E., Iriarte, J. L., Tapia, F. J., Lizarraga, L., ... and Pizarro, O.: Seasonal variability of primary production in a fjord ecosystem of the Chilean Patagonia: Implications for the transfer of carbon within pelagic food webs, Continental Shelf Research, 31, 3-4, 202-215, doi:10.1016/j.csr.2010.09.003, 2011.

Montero, P., Pérez-Santos, I., Daneri, G., Gutiérrez, M. H., Igor, G., Seguel, R., ... and Crawford, D. W.: A winter dinoflagellate bloom drives high rates of primary production in a Patagonian fjord ecosystem, Estuarine, Coastal and Shelf Science, 199, 105-116, doi:10.3856/vol45-issue5-fulltext-16, 2017.

Montero, P., Daneri, G., Tapia, F., Iriarte, J. L., and Crawford, D.: Diatom blooms and primary production in a channel ecosystem of central Patagonia, Lat. Am. J. Aquat. Res. 45, 999–1016, doi: 10.3856/vol45-issue5-fulltext-16, 2017a.

Montero, P., Gutiérrez, M. H., Daneri, G., and Jacob, B.: The Effect of Salmon Food-Derived DOM and Glacial Melting on Activity and Diversity of Free-Living Bacterioplankton in Chilean Patagonian Fjords, Frontiers in Microbiology, 12, 772900, doi:10.3389/fmicb.2021.772900, 2022

Nimptsch, J., Woelfl, S., Osorio, S., Valenzuela, J., Ebersbach, P., von Tuempling, W., ... and Graeber, D.: Tracing dissolved organic matter (DOM) from land-based aquaculture systems in North Patagonian streams, Science of the Total Environment, 537, 129-138, doi:10.1016/j.scitotenv.2015.07.160, 2015.

Oschlies, A., Brandt, P., Stramma, L., and Schmidtko, S.: Drivers and mechanisms of ocean deoxygenation, Nature Geoscience, 11, 7, 467-473, doi:10.1038/s41561-018-0152-1, 2018.

Paulmier, A., and Ruiz-Pino, D.: Oxygen minimum zones (OMZs) in the modern ocean, Progress in Oceanography, 80, 3-4, 113-128, doi:10.1016/j.pocean.2008.08.001, 2009.

Pawlowicz, R., Beardsley, B., Lentz, S.: Classical tidal harmonic analysis including error estimates in MATLAB using T_TIDE. Comput. Geosci. 28, 929–937. https://doi.org/10.1016/S0098-3004(02)00013-4, 2002.

Pérez-Santos, I., Garcés-Vargas, J., Schneider, W., Ross, L., Parra, S., and Valle-Levinson, A.: Double-diffusive layering and mixing in Patagonian fjords, Progress in Oceanography, 129, 35-49, doi:10.1016/j.pocean.2014.03.012, 2014.

Pérez-Santos, I., Castro, L., Ross, L., Niklitschek, E., Mayorga, N., Cubillos, L., ... and Daneri, G.: Turbulence and hypoxia contribute to dense biological scattering layers in a Patagonian fjord system, Ocean Science, 14, 5, 1185-1206, doi:10.5194/os-14-1185-2018, 2018.

Pérez-Santos, I., Díaz, P., Silva, N., Garreaud, R., Montero, P., Henríquez-Castillo, C., Barrera, F., Linford, P., Amaya, C., Contreras, S., Aracena, C., Pinilla, E., Altamirano, R., Vallejos, L., Pavez, J., and Maulen, J.: Oceanography time series reveals annual asynchrony input between oceanic and estuarine waters in Patagonian fjords. Sci. Total Environ. 798, 149241. doi.org/10.1016/j.scitotenv.2021.149241, 2021.

Pinilla, E., Castillo, M. I., Pérez-Santos, I., Venegas, O., and Valle-Levinson, A.: Water age variability in a Patagonian fjord, Journal of Marine Systems, 210, 103376, doi:10.1016/j.jmarsys.2020.103376, 2020.

Pinilla, E., Soto, G., Arriagada, M., Canon, H.: Diseño y estudio técnico de macrozonas de agrupaciones de concesiones en la zona sur austral X a XII Regiones. Valparaíso, Instituto de Fomento Pesquero. Available: http://190.151.20.106/exlibris/aleph/a23_1/apache_media VB3VMRJKVR6S2C2IA2E1XGA85FQPPC.pdf, 2012.

Prandle, D.: Simple theory for designing tidal power schemes, Advances in water resources, 7, 1, 21-27, doi:10.1016/0309-1708(84)90026-5, 1984.

Quiñones, R. A., Fuentes, M., Montes, R. M., Soto, D., and León-Muñoz, J.: Environmental issues in Chilean salmon farming: a review, Reviews in Aquaculture, 11, 2, 375-402, doi:10.1111/raq.12337, 2019.

Rabalais, N. N., Díaz, R. J., Levin, L. A., Turner, R. E., Gilbert, D., and Zhang, J.: Dynamics and distribution of natural and human-caused hypoxia, Biogeosciences, 7, 585–619, https://doi.org/10.5194/bg-7-585-2010, 2010.

Remeikaitė-Nikienė, N., Lujanienė, G., Malejevas, V., Barisevičiūtė, R., Zilius, M., Vybernaitė-Lubienė, I., ... and Stankevičius, A.: Assessing nature and dynamics of POM in transitional environment (the Curonian Lagoon, SE Baltic Sea) using a stable isotope approach, Ecological Indicators, 82, 217-226, doi:10.1016/j.ecolind.2017.06.035, 2017.

Reche, P., Artal, O., Pinilla, E., Ruiz, C., Venegas, O., Arriagada, A., Falvey, M.: CHONOS: oceanographic information website for Chilean Patagonia. Ocean Coast Manag. 208, 105634 https://doi.org/10.1016/j.ocecoaman.2021.105634, 2021.

Redfield A. C.: The biological control of chemical factors in the environment. Am. Sci., 46:230A-A221, 1958.

Robinson, C.: Microbial respiration, the engine of ocean deoxygenation, Frontiers in Marine Science, 5, 533, doi:10.3389/fmars.2018.00533, 2019.Rodi, W: In: Turbulence Models and Their Application in Hydraulics. Delft, p. 104, 1984.

Rosentreter et al.: Coastal vegetation and estuaries are collectively a greenhouse gas sink, Nature climate change, https://doi.org/10.1038/s41558-023-01682-9, 2023.

Rosen S., Bianucci L., Jackson J.M., Hare A., Greengrove C., Monks R., Bartlett M. and Dick J.: Seasonal near-surface hypoxia in a temperate fjord in Clayoquot Sound, British Columbia. Front. Mar. Sci. 9:1000041. doi: 10.3389/fmars.2022.1000041, 2022.

Ruiz, C., Artal, O., Pinilla, E., and Sepúlveda, H. H.: Stratification and mixing in the Chilean Inland Sea using an operational model, Ocean Modelling, 158, 101750, doi:10.1016/j.ocemod.2020.101750, 2021.

Sampaio, E., Santos, C., Rosa, I. C., Ferreira, V., Pörtner, H. O., Duarte, C. M., ... and Rosa, R.: Impacts of hypoxic events surpass those of future ocean warming and acidification, Nature Ecology and Evolution, 5, 3, 311-321, doi:10.1038/s41559-020-01370-3, 2021.

Saino, T., Hattori, A.:15N natural abundance in oceanic suspended particulate matter. Nature 283, 752–754, 1980.

Saino, T., Hattori, A.: Geographical variation of the water column distribution of suspended particulate nitrogen and its 15N natural abundance in the Pacific and its marginal seas. Deep-Sea Res. 34, 807–827, 1987.

Savoye, N., Aminot, A., Treguer, P., Fontugne, M., Naulet, N., and Kérouel, R.: Dynamics of particulate organic matter δ15N and δ13C during spring phytoplankton blooms in a macrotidal ecosystem (Bay of Seine, France). Mar Ecol-Progr Ser 255:27–41, 2003.

Schmidtko, S., Stramma, L., and Visbeck, M.: Decline in global oceanic oxygen content during the past five decades, Nature, 542, 7641, 335-339, doi:10.1038/nature21399, 2017.

Schneider, W., Pérez-Santos, I., Ross, L., Bravo, L., Seguel, R., and Hernández, F.: On the hydrography of Puyuhuapi Channel, Chilean Patagonia, Progress in Oceanography, 129, 8-18, doi:10.1016/j.pocean.2014.03.007, 2014.

Schneider, B., Schlitzer, R., Fischer, G. & Nothig, E. M.: Depth-dependent elemental compositions of particulate organic matter (POM) in the ocean. Glob. Biogeochem. Cycle https://doi.org/10.1029/2002gb001871, 2003.

Sibson, R., and Thomson, G. D.: A seamed quadratic element for contouring, The Computer Journal, 24, 4, 378-382, doi:10.1093/comjnl/24.4.378, 1981.Sievers, H. A.: Temperature and salinity in the austral Chilean channels and fjords. Progress in the oceanographic knowledge of Chilean interior waters, from Puerto Montt to Cape Horn. Comité Oceanográfico Nacional-Pontificia Universidad Católica de Valparaíso, Valparaíso, 31-36, 2008.

Sievers, A.H. and N. Silva.: Water masses and circulation in austral Chilean channels and fjords, In: N. Silva and S. Palma (eds.), Progress in the oceanographic knowledge of Chilean inner waters, from Puerto Montt to Cape Horn, Comité Oceanografico Nacional, Pontificia Universidad Católica de Valparaíso, Valparaíso, pp. 53-58. http://www.cona.cl/, 2008.

Silva, N.: Physical and chemical characteristics of the surface sediments in the austral Chilean channels and fjords, Progress in the oceanographic knowledge of Chilean interior waters, from Puerto Montt to Cape Horn, 69-75, http://www.cona.mil.cl/, 2008.

Silva, N., Rojas, N., and Fedele, A.: Water masses in the Humboldt Current System: Properties, distribution, and the nitrate deficit as a chemical water mass tracer for Equatorial Subsurface Water off Chile, Deep Sea Research Part II: Topical Studies in Oceanography, 56, 16, 1004-1020, doi:10.1016/j.dsr2.2008.12.013, 2009.

Silva, N., and Vargas, C. A.: Hypoxia in Chilean patagonian fjords, Progress in Oceanography, 129, 62-74, doi:10.1016/j.pocean.2014.05.016, 2014.

Smith, D. C., and Azam, F.: A simple, economical method for measuring bacterial protein synthesis rates in seawater using 3H-leucine, Mar. Microb. food webs, 6, 2, 107-114, 1992.

Sibson, R.: A Brief Description of Natural Neighbor Interpolation. In: Barnett, V., Ed., Interpreting Multivariate Data, John Wiley & Sons, New York, 21-36, 1981.

Soto, D., and Norambuena, F.: Evaluation of salmon farming effects on marine systems in the inner seas of southern Chile: a large-scale mensurative experiment, Journal of Applied Ichthyology, 20, 6, 493-501, doi:10.1111/j.1439-0426.2004.00602, 2004.

Soto, D., León-Muñoz, J., Garreaud, R., Quiñones, R. A., and Morey, F.: Scientific warnings could help to reduce farmed salmon mortality due to harmful algal blooms, Marine Policy, 132, 104705, doi:10.16/j.marpol.2021.104705, 2021.

Soto-Riquelme, C., Pinilla E., and Ross L.: Wind influence on residual circulation in Patagonian channels and fjords, Continental Shelf Research, 254, 104905, 2023.

Skamarock, W.C., Klemp, J.B., Dudhia, J., Gill, D.O., Barker, D.M., Duda, M.G., Huang, X.-Y., Wang, W., and Powers, J.G.: A description of the advanced research WRF version 3. NCAR Technical Note 475, 125, 2008.

Smagorinsky, J.: General circulation experiments with the primitive equations. Mon. Wea. Rev., 91, 99–164, 1963.

Stanton, B. R.: Some oceanographic observations in the New Zealand fjords, Estuarine, coastal and shelf science, 19, 1, 89-104, doi:10.1016/0272-7714(84)90054-4, 1984.

Stedmon, C., Norman, N.: Chapter 10 - The Optical Properties of DOM in the Ocean, Editor(s): Dennis A. Hansell, Craig A. Carlson, Biogeochemistry of Marine Dissolved Organic Matter (Second Edition), Academic Press, 2015, Pages 481-508, ISBN 9780124059405, https://doi.org/10.1016/B978-0-12-405940-5.00010-8, 2015.

Strickland, J. D. H.: Measuring the production of marine phytoplankton, Fish. Res. Bd. Canada Bull., 122, 172, 1960.

Strickland, J. D. H., and Parsons, T. E.: Determination of dissolved oxygen, A practical handbook of seawater analysis, 167, 71-75, 1968.

Takeoka, H.: Fundamental concepts of exchange and transport time scales in a coastal sea, Continental Shelf Research, 3, 3, 311-326, doi:10.1016/0278-4343(84)90014-1, 1984.

Taucher, J., Boxhammer, T., Bach, L. T., Paul, A. J., Schartau, M., Stange, P., & Riebesell, U.: Changing carbon-to-nitrogen ratios of organic-matter export under ocean acidification. Nature Climate Change. doi:10.1038/s41558-020-00915-5, 2020. Tomas, C. R. (Ed.).: Identifying marine phytoplankton, Elsevier, 1997.

Tomas, H., Ittekkot, V., Osterroht, C. & Schneider, B.: Preferential recycling of nutrients—the ocean's way to increase new production and to pass nutrient limitation? Limnol. Oceanogr. 44, 1999–2004, 1999.

Thomson, R.E., and Emery, W.J.: Data Analysis Methods in Physical Oceanography, Elsevier, Waltham, Mass. Paperback ISBN: 9780123877826, 2014.

Thomson, R.E., Spear, D.J., Krassovski, M.V., Hourston, R.A.S., Juhász, T.A., and Mihály, S.F.: Buoyancy-driven coastal current blocks ventilation of an anoxic fjord on the Pacific coast of Canada, J. Geophys. Res. Oceans, 122, 2976–2998, doi:10.1002/2016JC012512, 2017.

Torres, R., Pantoja, S., Harada, N., González, H. E., Daneri, G., Frangopulos, M., ... and Fukasawa, M.: Air-sea CO2 fluxes along the coast of Chile: From CO2 outgassing in central northern upwelling waters to CO2 uptake in southern Patagonian fjords, Journal of Geophysical Research: Oceans, 116, C9, doi:10.1029/2010JC006344, 2011.

Troupin, C., Machín F., Ouberdous M., Sirjacobs D., Barth A., and Becker J.-M.: High-resolution climatology of the northeast Atlantic using Data-Interpolating Variational Analysis (Diva), J. Geophys. Res., 115, C08005, doi:10.1029/2009JC005512, 2010.

Utermöhl, H.: Zur vervollkommnung der quantitativen phytoplankton-methodik: Mit 1 Tabelle und 15 abbildungen im Text und auf 1 Tafel, Internationale Vereinigung für theoretische und angewandte Limnologie: Mitteilungen, 9, 1, 1-38, doi:10.1018/05384680.1958.11904091, 1958.

Vanhellemont, Q., and Ruddick, K.: Atmospheric correction of metre-scale optical satellite data for inland and coastal water applications, Remote sensing of environment, 216, 586-597, doi:10.1016/j.rse.2018.07.015, 2018.

Vaquer-Sunyer, R., and Duarte, C. M.: Thresholds of hypoxia for marine biodiversity, Proceedings of the National Academy of Sciences, 105, 40, 15452-15457, doi:10.1073/pnas.0803833105, 2008.

Valdenegro, A., and Silva, N.: Caracterizacion oceanografica física y química de la zona de canales y fiordos australes de Chile entre el estrecho de Magallanes y cabo de Hornos (CIMAR 3 fiordo). Cienc. Tecnol. del Mar 26 (2), 19–60, 2003.

Verardo, D. J., Froelich, P. N., and McIntyre, A.: Determination of organic carbon and nitrogen in marine sediments using the Carlo Erba NA-1500 Analyzer, Deep Sea Research Part A. Oceanographic Research Papers, 37, 1, 157-165, doi:10.1016/0198-0149(90)90034-S, 1990.

Velinsky, D. J., and Fogel, M. L.: Cycling of dissolved and particulate nitrogen and carbon in the Framvaren Fjord, Norway: stable isotopic variations. Marine Chemistry, 67(3-4), 161–180. doi:10.1016/s0304-4203(99)00057-2, 1999.

Wang, X., Olsen, L. M., Reitan, K. I., and Olsen, Y.: Discharge of nutrient wastes from salmon farms: environmental effects, and potential for integrated multi-trophic aquaculture, Aquaculture Environment Interactions, 2, 3, 267-283, doi:10.3354/aei00044, 2012.

Williams, P. I., and Robertson, J. E.: Overall planktonic oxygen and carbon dioxide metabolisms: the problem of reconciling observations and calculations of photosynthetic quotients, Journal of plankton Research, 13, 153-169, doi:10.1093/oxfordjournals.plankt.a042366, 1991.

Yao, W., and Millero, F. J.: The chemistry of the anoxic waters in the Framvaren Fjord, Norway, Aquatic Geochemistry, 1, 53-88, 1995.

Zhang, J., Gilbert, D., Gooday, A.J., Levin, L., Naqvi, S.W.A., Middelburg, J.J., Scranton, M., Ekau, W., Peña, A., Dewitte, B., Oguz, T., Monteiro, P.M.S., Urban, E., Rabalais, N.N., Ittekkot, V., Kemp, W.M., Ulloa, O., Elmgren, R., Escobar-Briones, E. and Van der Plas, A.K.: Natural and human-induced hypoxia and consequences for coastal areas: synthesis and future development. Biogeoscience 7, 1443–1467, 2010. doi:10.5194/bg-7-1443-2010, 2010.